Haploinsufficiency of the ammonia transporter Rhcg predisposes to chronic acidosis. Rhcg is critical for apical and basolateral ammonia transport in the mouse collecting duct

Bourgeois, Soline ; Bounoure, Lisa ; Christensen, Erik I ; Ramakrishnan, Suresh K ; Houillier, Pascal ; Devuyst, Olivier ; Wagner, Carsten A

Abstract: Ammonia secretion by the collecting duct (CD) is critical for acid-base homeostasis and, when defective, causes distal renal tubular acidosis (dRTA). The Rhesus protein RhCG mediates NH(3) transport as evident from cell-free, cellular models, and Rhcg-null mice. Here we investigated in a Rhcg mouse model, the metabolic effects of Rhcg haploinsufficiency, the role of Rhcg in basolateral NH(3) transport, and mechanisms of adaptation to the lack of Rhcg. Both Rhcg(+/+) and Rhcg(+/-) mice were able to handle an acute acid load, whereas Rhcg(-/-) mice developed severe metabolic acidosis with reduced ammonuria and high mortality. However, chronic acid loading revealed that Rhcg(+/-) mice did not fully recover, showing lower blood HCO(3)(-) concentration and more alkaline urine. Microperfusion studies demonstrated that transepithelial NH(3) permeability was reduced by 80% and 40%, respectively, in CDs from Rhcg(-/-) and (+/-) mice compared to controls. Basolateral membrane permeability to NH(3) was reduced in CDs from Rhcg(-/-) mice consistent with basolateral Rhcg localization. Rhcg(-/-) responded to acid-loading with normal expression of enzymes and transporters involved in proximal tubular ammoniagenesis but reduced abundance of the NKCC2 transporter responsible for medullary accumulation of ammonium. Consequently, tissue ammonium content was decreased. These data demonstrate a role for apical and basolateral Rhcg in transepithelial NH(3) transport, uncover an incomplete dRTA phenotype in Rhcg(+/-) mice. Haploinsufficiency or reduced expression of RhCG may underlie human forms of (in)complete dRTA.

DOI: https://doi.org/10.1074/jbc.M112.441782

Haploinsufficiency of the ammonia transporter Rhcg predisposes to chronic acidosis

Rhcg is critical for apical and basolateral ammonia transport in the mouse collecting duct

Soline Bourgeois[1], Lisa Bounoure[1], Erik I. Christensen[2], Suresh K. Ramakrishnan[3,4], Pascal Houillier[3,5,6] Olivier Devuyst[1], Carsten A. Wagner[1]

[1]Institute of Physiology and ZHIP, University of Zurich, Zurich, Switzerland, [2]Department of Biomedicine, University of Aarhus, Aarhus, Denmark; [3]INSERM, Centre de Recherche des Cordeliers, UMRS872, Paris, France; [4]Université Pierre et Marie Curie, Faculté de Médecine, Paris, France; [5]Université Paris-Descartes, Paris, France; and [6]Hôpital Européen Georges Pompidou, Département de Physiologie, Assistance Publique-Hôpitaux de Paris, Paris, France.

Running title: Incomplete dRTA in *Rhcg* targeted mice

To whom correspondence should be addressed: Carsten A. Wagner, Institute of Physiology, University of Zurich, Winterthurerstrasse 190, CH-8057 Zurich, Switzerland, Tel.: +41-44-63 55023, Fax: +41-44-63 56814; E-mail: Wagnerca@access.uzh.ch

Keywords: Kidney, ammonia transport, Rhesus protein

Background: Rhesus proteins transport NH_3 and/or NH_4^+ in heterologous expression systems.
Results: Heterozygous Rhcg mice develop delayed metabolic acidosis whereas homozygous KO mice display severe metabolic acidosis. RhCG functions as NH_3 transporter on apical and basolateral membranes.
Conclusion: RhCG is a NH_3 but not NH_4^+ transporter.
Significance: Loss or reduced expression of *RhCG* may underlie inherited or acquired forms of human acidosis.

SUMMARY

Ammonia secretion by the collecting duct (CD) is critical for acid-base homeostasis and, when defective, causes distal renal tubular acidosis (dRTA). The Rhesus protein RhCG mediates NH_3 transport as evident from cell-free, cellular models, and Rhcg-null mice. Here we investigated in a *Rhcg* mouse model, the metabolic effects of Rhcg haploinsufficiency, the role of Rhcg in basolateral NH_3 transport, and mechanisms of adaptation to the lack of Rhcg. Both $Rhcg^{+/+}$ and $Rhcg^{+/-}$ mice were able to handle an acute acid load, whereas $Rhcg^{-/-}$ mice developed severe metabolic acidosis with reduced ammonuria and high mortality. However, chronic acid loading revealed that $Rhcg^{+/-}$ mice did not fully recover, showing lower blood HCO_3^- concentration and more alkaline urine. Microperfusion studies demonstrated that transepithelial NH_3 permeability was reduced by 80% and 40%, respectively, in CDs from $Rhcg^{-/-}$ and $^{+/-}$ mice compared to controls. Basolateral membrane permeability to NH_3 was reduced in CDs from $Rhcg^{-/-}$ mice consistent with basolateral Rhcg localization. $Rhcg^{-/-}$ responded to acid-loading with normal expression of enzymes and transporters involved in proximal tubular ammoniagenesis but reduced abundance of the NKCC2 transporter responsible for medullary accumulation of ammonium. Consequently, tissue ammonium content was decreased. These data demonstrate a role for apical and basolateral Rhcg in transepithelial NH_3 transport, uncover an incomplete dRTA phenotype in $Rhcg^{+/-}$ mice. Haploinsufficiency or reduced expression of RhCG may underlie human forms of (in)complete dRTA.

INTRODUCTION

Ammonium (NH_4^+) is the main component of urinary acid excretion. Renal synthesis and excretion of NH_4^+ rise in response to an acid load, allowing kidneys to regenerate bicarbonate and increase net acid excretion (for review (1 ,2)). Impaired renal acid excretion characterizes type I distal renal tubular acidosis (dRTA) with low urinary ammonium and inappropriately alkaline urinary pH (3).

Ammonium is formed in the proximal tubule from the metabolism of glutamine and added to the luminal fluid. It is reabsorbed into the medullary interstitium in the thick ascending limb (TAL) creating a cortico-papillary NH_3/NH_4^+ gradient (4-5). The final step of NH_3/NH_4^+ excretion is achieved by the CD (6). The high tissue concentration of NH_3/NH_4^+ and the pH gradient between interstitium and urine provide the driving forces for NH_4^+ excretion into urine. NH_4^+ secretion results from the trapping of NH_3 in the tubular lumen after being titrated by H^+ ions stemming from active secretion by V-type H^+-ATPases (7).

The mechanisms mediating NH_3/NH_4^+ transport across cell membranes into urine have only recently become uncovered. Members of the Rhesus protein family have been identified as pathways for NH_3/NH_4^+ transport in yeast, plants, fish, and mammals (2,5,8). In the kidney CD RhCG and RhBG, are expressed (9-10). Mice lacking *Rhbg* show either no phenotype or only a very mild reduction in urinary ammonium excretion (11-12). In contrast, cell-specific or complete *Rhcg* deficiency causes a massive reduction in urinary ammonium excretion in three different mouse models (13-15). Microperfusion experiments using CDs from *Rhcg* deficient mice demonstrated that RhCG is critical for the apical exit of NH_3 into urine (13). Thus far, a phenotype of dRTA has only been reported in $Rhcg^{-/-}$ mice, whereas potential changes caused by haploinsufficiency in Rhcg have not been investigated. This issue is relevant since heterozygous abnormalities in RhCG might be more frequent and may affect the renal capacity to cope with an acid load leading to incomplete dRTA. Furthermore, $Rhcg^{+/-}$ mice may also serve as a model to examine the consequences of reduced RhCG expression that may occur during kidney disease. Lastly, RhCG localization has been controversial for years. RhCG has been localized by some groups only at the apical side of CD cells whereas others have found RhCG on both apical and basolateral membranes (9-10,16-17). The functionality of basolateral RhCG protein remains unknown.

Here, we used a novel *Rhcg* mouse model to provide the first evidence that haploinsufficiency in *Rhcg* impairs the handling of a chronic acid load in $Rhcg^{+/-}$ mice, which develop an incomplete metabolic acidosis. Microperfusion studies provide the functional basis of the defect and show that RhCG is absolutely required for apical and partially for basolateral NH_3 transport. Moreover, loss of Rhcg is associated with a profound downregulation of NKCC2 and reduced medullary accumulation of ammonium impairing the gradient necessary for the final excretory step. These data provide new insights into the complex role of RhCG and suggest that congenital or acquired defects in *RhCG* protein expression may be associated with incomplete dRTA.

EXPERIMENTAL PROCEDURES

Animals - $Rhcg^{+/-}$ mice were purchased from the Texas Institute of Genomic Medicine (TIGM, Houston TX, USA). Mice were generated by replacing exon 1 by a vector carrying a LacZ/Neo cassette (fig. 1A). Mice were genotyped by PCR directly on a 3 µl 25 mM NaOH tail digestion product. Genomic DNA was amplified using primer pairs specific for exon 1: forward (AGACCCCACAATGGAAAGCTATAA) and wildtype reverse (CAACCAGAACTCCCCAGTGTCAGA) and Knock-out reverse (ATGGGCTGACCGCTTCCTCGTGCTTTAC). The products were separated by electrophoresis in 1% agarose gel (mutant product: 522 bp, wildtype product: 376 bp). Mice were generated by matting $Rhcg^{+/-}$ mice and were breeding in EOPS animal facility. For acid loading experiments, mice in metabolic cages were given 0.2 M HCl added to powdered standard food. All experiments were performed according to Swiss Animal Welfare laws and approved by the local veterinary authority (Veterinäramt Zürich).

In vivo experiments - All experiments were performed using age- and sex-matched *Rhcg* wildtype ($Rhcg^{+/+}$), *Rhcg* knockout ($Rhcg^{-/-}$), and *Rhcg* heterozygote ($Rhcg^{+/-}$) littermate mice (3-4 month-old), housed in metabolic cages (Techniplast, Switzerland). Mice were given deionized water ad libitum and were fed with a standard powdered laboratory chow (Kliba, Augst, Switzerland). Mice were allowed to adapt to metabolic cages for 3 days and a first retro-orbital blood sample was taken for blood gas analysis under baseline. Then two 24 hrs urine samples were collected under light mineral oil in the urine collector to determine daily urinary parameters. Mice were then allowed to recover for 2 weeks before given a HCl-containing diet (0.2 M HCl added to powdered standard food) in normal cages. Food, water intake, and urine excretion was monitored following the same procedures as under baseline conditions. Urine collections were performed on the first and second day of acid-loading, and then on the sixth and seventh day. Retro-orbital blood sample was taken on second and seventh days HCl diet.

Analytic procedures - Blood pH, PCO_2, and electrolytes were measured with a pH/blood-gas analyzer (ABL 77 Radiometer). Urinary Na^+ and K^+ concentrations were measured by flame photometry (IL943, Instruments Laboratory), titratable acid were measured using a DL 50 titrator (Mettler Toledo (18-19) and creatinine by a modified kinetic Jaffé colorimetric method (20). Urinary pH and bicarbonate were measured with a pH/blood-gas analyzer (ABL 725, Radiometer). Urinary NH_4^+ was measured with the Berthelot protocol (21).

Immunoblotting – Crude membrane proteins or cytosolic fractions were obtained from kidneys homogenized in 250 mM sucrose, 10 mM Tris-HCl, pH 7.5, and in the presence of protease inhibitors.
Fourty micrograms of crude membrane proteins or cytosolic proteins were solubilized in loading buffer containing DTT and separated on 8 to 10% polyacrylamide gels. For immunoblotting, the proteins were transferred electrophoretically to polyvinylidene fluoride membranes (Immobilon-P, Millipore Corp., Bedford, MA, USA). After blocking with 5 % milk powder in Tris-buffered saline/0.1% Tween-20 for 60 min, the blots were incubated with primary antibodies: phosphate-dependent glutaminase (PDG), which recognizes both the rat (KGA) and human (GAC) kidney-type isoforms of PDG forming the mature PDG protein (66 and 68 kDa; a kind gift from N. Curthoys, Colorado State University, USA; diluted 1:5000) (22), rabbit polyclonal anti-PEPCK (Cayman Chemical, Ann Arbor, MI; diluted 1:5,000), rabbit polyclonal anti-NKCC2 (kind gift from Johannes Loffing, Institute of Anatomy, Univ. of Zurich; diluted 1:5,000), rabbit polyclonal anti-NHE3 (StressMarq Biosciences Inc., Victoria, BC, Canada), rabbit polyclonal anti-pendrin (Pineda Antibody Service, Berlin, Germany, 1:5,000 (23) and mouse monoclonal anti-β-actin antibody (Sigma, St. Louis, MO; 1:5,000) overnight at 4°C. After washing and blocking with 5 % milk powder for 60 min, membranes were then incubated for 2 h at

room temperature with secondary goat anti-rabbit or donkey anti-mouse antibodies 1:5,000 linked to alkaline phosphatase (Promega, Madison, WI, USA). The protein signal was detected with the appropriate substrate (Millipore Corp, Bedford, MA, USA) using the las-4000 image analyzer system (Fujifilm Life Science USA). All images were analyzed using the software Advanced Image Data Analyzer AIDA (Raytest, Straubenhardt, Germany) to calculate the protein of interest/β-actin ratio.

Immunostaining and immunogold - Immunohistochemistry and immunogold staining were performed on frozen sections, and specificity was demonstrated on *Rhcg*$^{-/-}$ tissues. Mouse kidneys were fixed by perfusion retrograde through the aorta with 3% paraformaldehyde in 0.1 M sodium cacodylate buffer, pH 7.2. The tissue was either trimmed into small blocks, further fixed by immersion in 1% paraformaldehyde, infiltrated with 2.3 M sucrose for 30 min and frozen in liquid nitrogen or prepared for routine paraffin embedding. For electron microscopy 70-90 nm cryosections were obtained at -100^{o}C with an FCS Reichert Ultracut S cryoultramicrotome as previously described (24) and 2 µm paraffin sections were obtained with a Leica RM2165 microtome. For LM immunolabeling, the sections were incubated with a rabbit polyclonal antibody against RhCG (a kind gift from Dr. Yves Colin, INSERM Paris (16,25)) at room temperature for 1 hr after preincubation in PBS containing 0.05 M glycine and 1% bovine serum albumin. The sections were subsequently incubated with peroxidase-conjugated secondary antibody (Dako), the peroxidase was visualized with diaminobenzidine and the sections were counter stained with Maier´s stain for 2 min. The sections were examined in a Leica DMR microscope equipped with a Leica DFC320 camera. Images were transferred by a Leica TFC Twain 6.1.0 program and processed using Adobe Photoshop 8.0. For EM immunolabeling the section were incubated with the primary antibody at 4^{o}C over night followed by incubation at room temperature for 1 hour with 10 nm gold particles coupled to anti-rabbit IgG (BioCell, Cardiff, UK). The cryosections were embedded in methylcellulose containing 0.3% uranyl acetate and studied in a Philips CM100 electron microscope. Controls. Sections were incubated with secondary antibodies alone or with non-specific IgG.

RNA extraction and reverse transcription - Snap-frozen kidneys (five kidneys for each condition) were homogenized in RLT-Buffer (Qiagen, Basel, Switzerland) supplemented with β-mercaptoethanol to a final concentration of 1%. Total RNA was extracted from 200 µl aliquots of each homogenized sample using the RNeasy Mini Kit (Qiagen,Basel, Switzerland) according to the manufacturer's instructions. Quality and concentration of the isolated RNA preparations were analyzed on the ND-1000 spectrophotometer (Nano-Drop Technologies). Total RNA samples were stored at−80°C. Each RNA sample was diluted to 100 ng/µl and 3 µl used as a template for reverse transcription using the TaqMan Reverse Transcription Kit (Applied Biosystems, Forster City, CA, USA). For reverse transcription, 300 ng of RNA template were diluted in a 40-µl reaction mix that contained (final concentrations) RT buffer (1×), $MgCl_2$ (5.5 mM), random hexamers (2.5 µM), RNase inhibitor (0.4U/µl), the multiscribe reverse transcriptase enzyme (1.25U/µl), dNTP mix (500 µM each), and RNase-free water.

Real-time quantitative PCR - Quantitative real-time qRT-PCR was performed on the ABI PRISM 7700 Sequence Detection System (Applied Biosystems, Forster City, CA). Primers were chosen using BLAST tool of Ensemble (http://www.ensembl.org/index.html) to result in amplicons no longer than 150 bp spanning intron-exon boundaries to exclude genomic DNA contamination The specificity of all primers was first tested on mRNA derived from kidney and always resulted in a single product of the expected size (data not shown). Probes were labeled with the reporter dye FAM at the 5' end and the quencher dye TAMRA at the 3' end (Microsynth, Balgach, Switzerland). The primers were designed to target the deleted sequence in *Rhcg*$^{-/-}$ animals (accession number NM_019799) with 5' ATGCAGGGATGGTTCCATTA 3' [238-258 bp] as the left primer located within exon 1 and 5' TGGAAGAAGGTCATAATGAGCAG 3' [373-392 bp] as the right primer located within exon 2, and 5' TTACTATCGCTACCCGAGCTTCCAG 3' as the probe [292-317 bp]. Real-Time PCR reactions were performed using TaqMan Universal PCR Master Mix (Applied Biosystems, Forster City, CA). Briefly, 3 µl cDNA, 0.8 µl of each primer (25 µM), 0.4 µl labeled probe (5 µM), 5 µl RNAse-free water, and 10 µl TaqMan Universal PCR Master Mix reached 20 µl of final reaction volume. Reaction conditions were denaturation at 95°C for 10 min followed by 40 cycles of denaturation at 95°C for 15s and annealing/elongation at 60°C for 60s with auto ramp time. All reactions were run in triplicate. For analyzing the data, the threshold was set to 0.2 as this value had been determined to be in the linear range of the amplification curves for all mRNAs in all

experimental runs. The expression of the genes of interest was calculated in relation to hypoxanthine guanine phosphoribosyl transferase (HPRT, accession number: NM_013556, forward primer: 5′TTATCAGACTGAAGAGCTACTGTAAGATC-3′ (442–471), reverse ′ primer: 5 - TTACCAGTGTCAATTATATCTTCAACAATC-3′ (539–568), ′ probe: 5 - TGAGAGATCATCTCCACCAATAACTTTTATGT CCC-3′ (481–515)). Relative expression ratios were calculated as $R = 2^{(Ct(HPRT) - Ct(test\ gene)}$, where Ct represents the cycle number at the threshold 0.02.

Measurement of renal ammonia content - The renal tissue ammonia content was measured by an enzymatic technique (Ammonia Assay Kit, Sigma, Buchs, Switzerland) as previously described (26). Mice were anesthetized and the kidneys were removed and immediately frozen in liquid nitrogen. They were then sliced frozen to yield a column of tissue, which extended from the cortex to the tip of the papilla. Sections were cut along the corticomedullary axis to yield 3 slices: cortex, outer medulla, and inner medulla. Two kidneys from the same animal were pooled for each sample. Tissue slices were then homogenized in 300 µl of ice cold 7 % trichloroacetic acid, and the solution was centrifuged. The supernatant was drawn off and the pH of a 250 µl sample was adjusted to near neutral by the addition of 12 µl of 10 mM Na_2HPO_4 in 9 N NaOH. A 200 µl sample of buffered supernatant was then analyzed for ammonium. The pellet was resuspended in 1 N NaOH, shaken overnight, and analyzed for total protein using the Biorad protein assay.

Microperfusion studies on isolated tubules - Mice were anesthetized with 50 mg/kg pentobarbital sodium or Xylazin/Ketamin i.p. Both kidneys were cooled *in situ* with control bath solution (see below) for 1 min and then removed and cut into thin coronal slices for tubule dissection. Cortical CDs (CCDs) were dissected from the cortex at 10°C in the control solution. In vitro microperfusion of single CCD segments, intracellular pH, and transepithelial NH_3 permeability measurements were performed as described previously (13).

Intracellular pH measurement - The isolated tubule was transferred to the bath chamber on the stage of an inverted microscope (Axiovert 200, Carl Zeiss, Germany) in the control solution containing (in mM) 138 NaCl, 1.5 $CaCl_2$, 1.2 $MgSO_4$, 2 K_2HPO_4, 10 HEPES, 5.5 glucose, 5 alanine, pH 7.40) and then, was mounted on concentric pipettes and perfused *in vitro* with Na^+-free, ammonium-free solution where N-methyl-D-Glutamine$^+$ ($NMDG^+$) replaced Na^+. All solutions were equilibrated with 100% O_2 passed through a 3 N KOH CO_2 trap. Once the solutions were gassed and the pH checked, they were placed in a reservoir and were continuously bubbled with 100% O_2. The average tubule length exposed to bath fluid was limited to 300 – 350 µm in order to prevent motion of the tubule. CCDs or OMCDs were loaded with 5 µM of the fluorescent probe BCECF (2',7'-bis(2-carboxyl)-5-(and-6)-carboxyfluorescein, Invitrogen, Switzerland) for ~20 min at 37°C in the control bath solution. The loading solution was then washed out by initiation of bath flow and the tubule was equilibrated with dye-free control bath solution for 5 min. Bath solution was delivered at a rate of 20 ml/min and warmed to 37°C by water jacket immediately upstream to the chamber. After this temperature equilibration in control solution, tubules were first transiently acidified by peritubular Na^+ removal (Na-free, ammonium-free solution) (10 min duration), replaced by $NMDG^+$ to avoid exit of NH_4^+ by basolateral Na^+-coupled transport. This maneuver was done in the luminal absence of Na^+. During the fluorescence recording, perfusion solution was delivered to the perfusion pipette via a chamber under an inert gas (N_2) pressure (around 1 bar) connected through a manual 6-way valve. With this system, opening of the valve instantaneously activates flow of solutions. The majority of the fluid delivery to the pipette exits the rear of the pipette system through a drain port at 4 ml/min. This method results in a smooth and complete exchange of the luminal or the peritubular solution in less than 3 to 4 s (27). After the fluorescence signal stabilization, luminal medium was instantly (at the rate of 4 ml/min in the draining) replaced by a Na^+-free solution containing 20 mM NH_4Cl (and 118 mM NMDG-Cl) that elicited a rapid intracellular alkalinization, followed by a sharp acidification. The rate of intracellular alkalinization has been associated with the entry of NH_3 whereas the subsequent phase of intracellular acidification in the continued presence of extracellular NH_4Cl reflects mostly NH_4^+ entry (28). Fluorescence monitoring and calibration were performed with a video imaging system (Visitron Systems, Germany) as previously described (11,13). For peritubular ammonium pulse, peritubular solution was changed by a 6 mM NH_4Cl solution, pH 7.40 in the presence of 1 mM furosemide and 2.5 mM ouabain in the bath.

Intrinsic buffering capacity determination - The intrinsic buffering capacity (ßi) of CCD cells was determined, as previously reported (29), using a 40 mM NH_4Cl basolateral pulse to acidify the cells. To

exclude HCO_3^-/CO_2 as a buffering component and block Na^+-dependent pH_i regulatory mechanisms, Na^+-free, HEPES-buffered solutions were used in perfusate and the bath contained 1 mM amiloride (to inhibit Na^+/H^+-exchangers) and bath and perfusate also contained 100 µM Sch28080 (to block H^+/K^+-ATPases) and 200 nM Concanamycin A (to block H^+-ATPases). Addition of 40 mM NH_4Cl to the bath induced an increase following by a decrease in pH_i. The pKa of ammonia (9.03) was used to calculate the intracellular NH_4^+ concentration when cell acidification plateaued. ßi was calculated as the ratio of the change in intracellular NH_4^+ concentration to the change in pH_i. Therefore, we determined the correlation between intracellular pH and β_I which was -32.7-22.3*pH in wildtypes, -2.3-8.2*pH in heterozygotes, and 1,4-5.0*pH_i in *Rhcg*$^{-/-}$ mice. We measured cellular buffering power (β_i) in CCDs from all three genotypes of mice.

NH_3 permeability measurement - The basic approach used to determine NH_3 permeability involved construction of a transepithelial gradient of NH_3 and measurement of the resulting NH_3 flux from the basolateral to the luminal side as previously described (11,13,30). The isolated CCD was transferred to the bath chamber on the stage of an inverted microscope (Axiovision A1, Zeiss, Germany) and mounted on concentric glass pipettes for microperfusion. Bath solution was delivered at a rate of 20 ml/min and warmed to 37°C by a water jacket immediately upstream of the chamber. The perfusion rate was adjusted by hydrostatic pressure to ~10 nl/min. The tubules were equilibrated for 20–30 min at 37°C before the beginning of collections. To construct a transepithelial NH_3 gradient, the perfusion (lumen) solution contained (in mM) 139 NaCl, 1 NH_4Cl, 2.5 K_2HPO_4, 2 $NaHCO_3$ (pH 6.4), the bath solution contained (in mM) 117 NaCl, 1 NH_4Cl, 2.5 K_2HPO_4, 23 $NaHCO_3$ (pH 7.4), in addition, both solutions contained (in mM) 5.5 glucose, 2 $CaCl_2$, 1.2 $MgSO_4$ and 10 HEPES. The osmolarity of the solution was 295 ± 5 mosmol/kg H_2O. All solutions were equilibrated with 95% O_2-5% CO_2. Once the solutions were gassed and the pH checked, they were placed in a reservoir and continuously bubbled with 95% O_2-5% CO_2. The actual pH of the solutions was monitored several times during experiments, and the pH of solutions was checked at the end of the experiment to ensure that changes did not occur. Carbonic anhydrase (Sigma, France) was added to the perfusate solution (1 mg/10 ml of solution). The purpose of carbonic anhydrase was to prevent any pH disequilibrium that might arise from proton secretion or NH_3 transport. Total ammonium concentration was measured in 10- to 12-nl samples of peritubular, perfused, and collected fluids using an NH_3 diagnostic kit (Sigma, France) and the flow-through microfluorometer Nanoflo apparatus (World Precision Instruments, UK) (31).

Calculations of transepithelial NH_3 permeability - Assuming an absence of osmotic or hydrostatic pressure gradients across the epithelium and therefore an absence of net fluid transport, the passive transepithelial transport of total ammonium (Am) may be described by

$$J_{Am} = P_{NH3} \times A_s \times \Delta C_{NH3}$$

where P_{NH3} is diffusive permeability of NH_3 (cm/s), A_s is tubule luminal surface area (cm^2), and ΔC_{NH3} is the transepithelial concentration difference for NH_3 (mM). To calculate the permeability to NH_3, the equation is rearranged as follows

$$P_{NH3} = J_{Am} / (A_s \times \Delta C_{NH3})$$

The net rate of transport J_{Am} is calculated as follows

$$J_{Am} = ([Am]_i - [Am]_o) \times V/L$$

where $[Am]_i$ is the concentration of total ammonium in the perfusate, $[Am]_o$ is the concentration of total ammonium in the collected fluid, V is the collection rate (nl/min), as measured in precalibrated constriction pipettes, and L is the perfused tubule length (mm). A_s may be calculated as $L\pi d$, where d (mm) is the inner tubule diameter. The total ammonium concentration ([Am]) is equal to the sum of the concentrations of the two species NH_3 and NH_4^+ and is the quantity actually measured by the microfluorimetric assay. The equilibrium between the two species is defined by the Henderson-Hasselbalch equation

$$pH = pK_a + log\ ([NH_3]/(NH_4^+))$$

The pK_a equals 9.03 at physiological pH and temperature. Knowing the values for pH and [Am], the values for $[NH_3]$ and $[NH_4^+]$ may be determined simultaneously.

Statistics - Data are expressed as means ± SEM. Statistical comparisons were tested by ANOVA and Student's t-test using the Graphpad Prism software (GraphPad). P values < 0.05 were considered as statistically significant.

RESULTS

Deletion of Rhcg in mice

Mice lacking *Rhcg* were generated using gene trap technology in a mixed genetic background (129SvEvBrd, C57/BL6) (Figure 1A) and were purchased from the Texas Institute of Genomic

Medicine (32). *Rhcg* mRNA was undetectable in renal tissue from Rhcg knock-out ($Rhcg^{-/-}$) mice and reduced by approximately 50 % in heterozygous mice ($Rhcg^{+/-}$) mice (Figure 1B). RhCG protein was completely absent from the kidney of $Rhcg^{-/-}$ mice as confirmed by immunohistochemistry (Figure 1C).

Heterozygous mice develop metabolic acidosis while on long-term acid load

We first assessed acid-base status under basal conditions and during an acid load in *Rhcg* littermates. Throughout the study, food intake was similar in all three genotypes. At baseline, no difference in acid-base and electrolyte levels was observed (Tables 1 and 2).

The effects of both acute (2 days) and chronic (7 days) HCl load were tested (Tables 1, 2 and 3, Figure 2). On the second day of the HCl load, blood pH and HCO_3^- concentration were decreased in all genotypes, as compared with baseline (Table 1, and Figure 2D and E). Blood pH and HCO_3^- concentration were significantly lower in $Rhcg^{-/-}$ mice but similar in $Rhcg^{+/-}$ and $Rhcg^{+/+}$ mice. Urinary ammonium excretion rate increased significantly on the first day of acid loading in $Rhcg^{+/+}$ and $Rhcg^{+/-}$ mice but much less in $Rhcg^{-/-}$ mice (Tables 2 and 3 and Figure 2A). Urinary pH decreased in $Rhcg^{+/+}$ and $Rhcg^{+/-}$ mice as compared to baseline values (Table 2 and Figure 2B) but to a lesser extent in $Rhcg^{-/-}$ mice. Urinary titratable acid excretion was unaltered in all three genotypes during the acute acid load. Long-term HCl loading resulted in the death of most $Rhcg^{-/-}$ mice, which poorly excreted ammonium and exhibited a very severe metabolic acidosis. These animals showed a higher loss of body weight after the acute HCl load presumably due to dehydration (Table 3).

In contrast to the $Rhcg^{+/+}$ mice, which adapted and nearly normalized their blood pH and HCO_3^- concentration, $Rhcg^{+/-}$ remained acidotic at day 7 of the HCl load – even though both genotypes maintained a high NH_4^+ excretion. At the end of the chronic acid load, $Rhcg^{+/-}$ mice showed less increase in their titratable acid excretion, and had a more alkaline urine pH (Tables 1 and 2 and Figure 2B and C). Thus, both $Rhcg^{-/-}$ and $Rhcg^{+/-}$ exhibited renal acid handling defects.

The absence of* RhCG *abolishes medullary ammonium accumulation

To assess the cortico-papillary gradient of NH_3/NH_4^+ in kidneys from *Rhcg* mice, we measured ammonium content in the cortex, outer and inner medulla after 4 days of HCl treatment. There was no difference between $Rhcg^{+/+}$ and $Rhcg^{+/-}$ mice. However, the inner medulla ammonium content was strongly reduced to 39% in $Rhcg^{-/-}$ mice (Figure 3). Thus, the absence of *Rhcg* impairs the ability to concentrate ammonium in the interstitium of the inner medulla.

RhCG is located at the apical and basolateral sides of cells along the distal nephron

RhCG has been localized to most cells of the CD including type A intercalated cells as well as principal cells (9,17). However, the subcellular localization of RhCG has remained controversial since some groups reported both apical and basolateral staining (10,17) whereas others detected only apical staining for RhCG (9) based on different immunohistochemical methods. We confirmed a strong labeling of both apical and basolateral poles of CD cells in mouse kidneys (Figure 4 and Table 4). This staining was absent from $Rhcg^{-/-}$ kidneys demonstrating its specificity. In the kidney cortex, RhCG was localized in DCT, CNT, and CCD (Figure 4A). In DCT cells, RhCG was mainly present at the apical side (Figure 4A). In CNT, CCD and OMCD, both intercalated and principal cells were stained. Principal cells and some intercalated cells exhibited RhCG staining at both the apical and basolateral sides (Figure 4A-C). However, in some cells RhCG was strictly localized at the apical pole (see arrows in Figure 4A, B, and D). These cells have been previously identified as non-A/non-B type intercalated cells (33-34). Finally, in the inner medulla, only strong apical and faint basolateral staining were found in intercalated cells (Figure 4D, Table 4). Immunogold electron microscopy demonstrated RhCG associated with the apical membrane as well as the basolateral interdigitations of segment specific and intercalated cells (Figure 4E and F). No specific immunogold labeling was found in kidneys from $Rhcg^{-/-}$ mice (data not shown). Thus, RhCG protein is expressed on both apical and basolateral membranes in mouse segment specific principal and intercalated CD cells.

Total and apical membrane permeabilities for NH_3 are reduced in CDs from $Rhcg^{+/-}$ mice

We assessed total transepithelial permeability for NH_3 in *in vitro* microperfused cortical CDs from *Rhcg* mice after a 2-day HCl diet, a condition causing a strong difference in urinary ammonium excretion between $Rhcg^{+/+}$ and $Rhcg^{-/-}$ mice. Imposing a bath-to-lumen NH_3 gradient in the nominal absence of an NH_4^+ gradient generated a measurable NH_3 secretory flux, which was significantly lower in CCDs from $Rhcg^{+/-}$ and $Rhcg^{-/-}$ mice vs. $Rhcg^{+/+}$ mice. These differences were due to a decrease in transepithelial

permeability to NH_3 by 54 % and 83 %, respectively (Table 5 and Figure 5). Thus, one *Rhcg* allele is not sufficient to sustain normal transepithelial permeability to NH_3 in the mouse collecting duct.

Next, we tested whether the apical permeability to NH_3 is affected in CDs from *Rhcg*$^{+/-}$ mice. Therefore, we measured the effects of an inwardly directed gradient on pHi on CCDs isolated from *Rhcg*$^{+/+}$ and *Rhcg*$^{+/-}$ mice (13). Figure 6A depicts the typical time course of pH_i changes when NH_3/NH_4^+ was added to the lumen tubule. The initial rate of cellular alkalinisation is proportional to the rate of apical NH_3 entry as previously described (13,35-36). In order to directly compare transport rates we measured intracellular buffering power and calculated the amount of H^+ used to titrate NH_3 transported across the membrane. Figure 6B depicts the calculated rate of NH_3 transported into CDs from *Rhcg*$^{+/+}$ and *Rhcg*$^{+/-}$ mice which was drastically reduced in *Rhcg*$^{+/-}$ tissue.

Basolateral RhCG accounts for peritubular membrane permeability to NH_3

Since RhCG is expressed at both sides of at least a subset of CD cells (Figure 4 and Table 4), we next tested the effect of *Rhcg* disruption on NH_3 transport across the basolateral membranes of CCD cells. Several transport pathways for NH_4^+ have been proposed at the basolateral side of CD cells including the Na^+-K^+-$2Cl^-$ cotransporter NKCC1 and the Na/K-ATPase where NH_4^+ would substitute for K^+ (37-38). Therefore, we performed experiments in the nominal absence of sodium to block the activity of both transport pathways.

Peritubular NH_3/NH_4^+ prepulses were performed on cortical CDs from *Rhcg*$^{+/+}$, *Rhcg*$^{+/-}$ and *Rhcg*$^{-/-}$ mice submitted to HCl loading for 2 days. As summarized in Figure 7, when NH_3/NH_4^+ (6 mM) was applied to the basolateral side the calculated rate of NH_3 transport into CD cells was unchanged in Rhcg$^{+/-}$ tissue but strongly reduced in *Rhcg*$^{-/-}$ tissue.

.

Thus, RhCG sustains both apical and basolateral transport of NH_3 in CD cells, in agreement with structural data and reconstituted RhCG suggesting that the protein forms a NH_3-permeable channel (39-40).

Compensatory adaptations to the loss of Rhcg

We finally examined whether *Rhcg deletion* affects mechanisms involved in renal ammoniagenesis and ammonium excretion. Surprisingly, immunoblots of whole kidney extracts from mice subjected to a 2-day HCl load revealed no differences in the expression of phosphoenolpyruvate carboxykinase (PEPCK) expression (Figure 8A). In contrast, the expression of the phosphate-dependent glutaminase (PDG), mediating the initial step of ammoniagenesis was decreased in *Rhcg*$^{+/-}$ kidneys as compared with both *Rhcg*$^{+/+}$ and *Rhcg*$^{-/-}$ kidneys (Figure 8B). The abundance of the Na^+/H^+ exchanger NHE3, involved in NH_4^+ secretion into the proximal tubule lumen, was unchanged (Figure 8C). Moreover, the expression of the Na^+-K^+-$2Cl^-$ cotransporter NKCC2, the main apical NH_4^+ transporter in the TAL, was highly downregulated in kidneys from *Rhcg*$^{+/-}$ and *Rhcg*$^{-/-}$ mice (Figure 8D).

DISCUSSION

Renal ammonium excretion is critical for acid-base homeostasis and is achieved by a complex process involving various nephron segments ((2,5-6)). A critical role for the Rhesus protein RhCG was demonstrated in tissue-specific and complete Knock-out mouse models (13-15). However, metabolic effects of *Rhcg* haploinsufficiency, the role of RhCG in basolateral NH_3 transport in CD cells, and the response of other pathways critical for renal ammoniagensis and ammonium transport have remained unknown. Based on a novel *Rhcg* mouse model, we show that *Rhcg* haploinsufficiency causes incomplete metabolic acidosis in mice. Secondly, RhCG contributes to peritubular NH_3 uptake giving functional evidence to the basolateral localization of RhCG in CD cells.

***Rhcg*$^{-/-}$ mice develop a severe incomplete renal tubular acidosis**

Rhcg$^{-/-}$ develop incomplete dRTA as evident from the inability to respond to an acute oral acid load. They showed severe hyperchloremic metabolic acidosis and did not increase urinary ammonium excretion resulting in low net acid excretion. Moreover, these animals had a drastic reduction in their blood HCO_3^- concentration and pH. *Rhcg*$^{-/-}$ mice developed severe dehydration as indicated by high blood hemoglobin and weight loss (Tables 2 and 4). These phenotypes are more pronounced than in mice with partial deletion of *Rhcg* (14-15).

***Rhcg* haploinsufficiency leads to metabolic acidosis**

Similarly, *Rhcg*$^{+/-}$ mice develop also an incomplete dRTA. However, these mice initially responded to the acid load by increasing urinary ammonium excretion to the same extent as *Rhcg*$^{+/+}$ mice. Later, they did not fully adapt to chronic acid-loading and remained acidotic after 7 days HCl

loading, being unable to correct blood HCO_3^- concentration and excreting more alkaline urine whereas total net acid excretion was comparable to *Rhcg*$^{+/+}$ animals. The incomplete chronic metabolic acidosis in *Rhcg*$^{+/-}$ mice is at least in part due to the inability to maximally acidify urine and to excrete adequate amounts of acid in the form of titratable acidity. The metabolic phenotype of *Rhcg*$^{+/-}$ mice was further supported by functional studies on microperfused CCDs. Transepithelial permeability to NH_3 was reduced in CCDs from *Rhcg*$^{-/-}$ and *Rhcg*$^{+/-}$ mice. The reduction in NH_3 permeability in CCDs from *Rhcg*$^{+/-}$ mice was less than in *Rhcg*$^{-/-}$ mice, suggesting that a 50% reduction in net NH_3 permeability in CCDs is still sufficient to support high ammonium excretion but is not enough to correct metabolic acidosis. Of note, medullary accumulation of NH_3/NH_4^+ appeared to be intact. Together, these results represent the first evidence that loss of a single *Rhcg* allele can lead to chronic hyperchloremic metabolic acidosis.

Renal adaptation to *Rhcg* invalidation

We further examined compensatory mechanisms in *Rhcg*$^{+/-}$ and *Rhcg*$^{-/-}$ mice. The generation of the cortico-papillary gradient of ammonium is required for the subsequent uptake of NH_3 and NH_4^+ by intercalated cells and the secretion of NH_3 into urine. Surprisingly, *Rhcg*$^{-/-}$ mice had low tissue ammonium content in the inner medulla after 4 days acid loading. This result suggests that the absence of RhCG affects the ability of the medulla to generate or maintain a high interstitium ammonium content. Since the key enzymes of proximal tubular ammoniagenesis, PEPCK and PDG were normally expressed in *Rhcg*$^{-/-}$ kidney tissue, mice most likely form adequate amounts of ammonium. In *Rhcg*$^{-/-}$ mice, this ammonium might be either shunted back into systemic circulation or not be absorbed at the level of the thick ascending limb.

Expression of NKCC2 was decreased in both *Rhcg*$^{+/-}$ and *Rhcg*$^{-/-}$ kidney tissues. NKCC2 is crucial for TAL NH_4^+ absorption and concentration in the medulla. Thus, our results suggest that mechanisms contributing to create a high medullary ammonium concentration are altered in Rhcg deficient mice. Other mechanisms such as increased removal of ammonium from the interstitium with venous blood might contribute also to the low medullary ammonium content. Metabolic acidosis alters concentrations of various vasoactive substances in the kidney, including higher levels of endothelin and prostaglandins and lower concentrations of NO (41-42), which may alter medullary blood flow and the kidneys ability to maintain the cortico-papillary ammonium gradient.

RhCG mediates NH_3 transport also at the basolateral side of CD cells

Subcellular RhCG localization has remained controversial for many years (9-10,17). Here, we confirmed a strong labeling of both apical and basolateral poles of CD cells in mouse kidneys. These data were corroborated by our functional study on in vitro microperfused CCDs. We measured a 60 % reduction in the NH_3 permeability at the basolateral side of *Rhcg*$^{-/-}$ CCD cells. This is the first evidence that Rhcg is also functional at the basolateral side of CDs cells and participates in basolateral NH_3 uptake. Hitherto it has been assumed that basolateral uptake occurs mostly if not exclusively in the form of NH_4^+ and that NH_3 plays no major role. Several pathways for NH_4^+ uptake have been delineated from pharmacological and functional experiments that demonstrated a role for the Na^+-K^+-$2Cl^-$ cotransporter NKCC1, the Na^+/K^+-ATPase, and possibly potassium channels where NH_4^+ always would replace potassium (37-38,43). We performed our experiments in the absence of sodium to reduce NKCC1 and Na^+/K^+-ATPase activity, respectively. Thus, our experiments do not allow concluding about the relative importance and contribution of these different pathways to total NH_3/NH_4^+ uptake across the basolateral membrane, but modify the current model of ammonium transport across the basolateral membrane. However it appears from the data on *Rhcg*$^{+/-}$ CCD that apical NH_3 flux critically depends on full RhCG expression whereas basolateral NH_3 flux is sustained with reduced RhCG expression suggesting that transport of NH_3 form is most important at the apical side. Finally, our findings could also explain the complete lack or only mild phenotype observed in *Rhbg* knock-out mice (11,44) where RhCG may have compensated for the lack of *RhBG*.

In summary, reduced expression or complete loss of expression of RhCG affect the kidneys ability to excrete acidic urine and appropriately regulate acid/base homeostasis. We provide the first functional evidence for basolateral RhCG activity and show that RhCG is expressed and functional on apical and basolateral membranes of most cells lining the renal collecting duct. Thus, *Rhcg* haploinsufficiency or *Rhcg* deletion may contribute to orphan forms of inherited distal renal tubular acidosis in humans as well as to acquired forms of dRTA.

Biobliography

1. Alpern, R. J., and Hamm, L. L. Urinary Acidification. in *Kidney* (Brenner, and Rector eds.). pp 23-40
2. Weiner, I. D., and Verlander, J. W. (2011) *Am J Physiol Renal Physiol* **300**, F11-23
3. Batlle, D. C., and Kurtzman, N. A. (1985) The defect in distal (type 1) renal tubular acidosis. in *Renal tubular disorders* (Gonick, H. C., and Buckalew, V. M. eds.). pp 281-305
4. Good, D. W. (1994) *Annu Rev Physiol* **56**, 623-647
5. Wagner, C. A., Devuyst, O., Belge, H., Bourgeois, S., and Houillier, P. (2011) *Kidney Int* **79**, 154-161
6. Wagner, C. A., Devuyst, O., Bourgeois, S., and Mohebbi, N. (2009) *Pflugers Arch* **458**, 137-156
7. Wagner, C. A., Finberg, K. E., Breton, S., Marshansky, V., Brown, D., and Geibel, J. P. (2004) *Physiol Rev* **84**, 1263-1314
8. DuBose, T. D., Jr., Good, D. W., Hamm, L. L., and Wall, S. M. (1991) *J Am Soc Nephrol* **1**, 1193-1203
9. Quentin, F., Eladari, D., Cheval, L., Lopez, C., Goossens, D., Colin, Y., Cartron, J. P., Paillard, M., and Chambrey, R. (2003) *J Am Soc Nephrol* **14**, 545-554
10. Brown, A. C., Hallouane, D., Mawby, W. J., Karet, F. E., Saleem, M. A., Howie, A. J., and Toye, A. M. (2009) *Am J Physiol Renal Physiol* **296**, F1279-1290
11. Chambrey, R., Goossens, D., Bourgeois, S., Picard, N., Bloch-Faure, M., Leviel, F., Geoffroy, V., Cambillau, M., Colin, Y., Paillard, M., Houillier, P., Cartron, J. P., and Eladari, D. (2005) *Am J Physiol Renal Physiol* **289**, F1281-1290
12. Bishop, J. M., Verlander, J. W., Lee, H. W., Nelson, R. D., Weiner, A. J., Handlogten, M. E., and Weiner, I. D. (2010) *Am J Physiol Renal Physiol*
13. Biver, S., Belge, H., Bourgeois, S., Van Vooren, P., Nowik, M., Scohy, S., Houillier, P., Szpirer, J., Szpirer, C., Wagner, C. A., Devuyst, O., and Marini, A. M. (2008) *Nature* **456**, 339-343
14. Lee, H. W., Verlander, J. W., Bishop, J. M., Igarashi, P., Handlogten, M. E., and Weiner, I. D. (2009) *Am J Physiol Renal Physiol* **296**, F1364-1375
15. Han, K. H., Lee, S. Y., Kim, W. Y., Shin, J. A., Kim, J., and Weiner, I. D. (2010) *Am J Physiol Renal Physiol* **299**, F187-198
16. Eladari, D., Cheval, L., Quentin, F., Bertrand, O., Mouro, I., Cherif-Zahar, B., Cartron, J. P., Paillard, M., Doucet, A., and Chambrey, R. (2002) *J Am Soc Nephrol* **13**, 1999-2008
17. Kim, H. Y., Verlander, J. W., Bishop, J. M., Cain, B. D., Han, K. H., Igarashi, P., Lee, H. W., Handlogten, M. E., and Weiner, I. D. (2009) *Am J Physiol Renal Physiol* **296**, F543-555
18. Jorgensen, K. (1957) *Scand J Clin Lab Invest* **9**, 287-291
19. Nutbourne, D. M. (1961) *Clin Sci* **20**, 263-278
20. Seaton, B., and Ali, A. (1984) *Med Lab Sci* **41**, 327-336
21. Berthelot, M. (1859) *Rep Chim App* **1**, 284
22. Curthoys, N. P., Kuhlenschmidt, T., Godfrey, S. S., and Weiss, R. F. (1976) *Arch Biochem Biophys* **172**, 162-167
23. Hafner, P., Grimaldi, R., Capuano, P., Capasso, G., and Wagner, C. A. (2008) *Am J Physiol Cell Physiol* **295**, C1658-1667
24. Christensen, E. I., Nielsen, S., Moestrup, S. K., Borre, C., Maunsbach, A. B., de Heer, E., Ronco, P., Hammond, T. G., and Verroust, P. (1995) *Eur J Cell Biol* **66**, 349-364
25. Marini, A. M., Matassi, G., Raynal, V., Andre, B., Cartron, J. P., and Cherif-Zahar, B. (2000) *Nat Genet* **26**, 341-344
26. Packer, R. K., Desai, S. S., Hornbuckle, K., and Knepper, M. A. (1991) *J Am Soc Nephrol* **2**, 77-83
27. Watts, B. A., 3rd, and Good, D. W. (1994) *J Biol Chem* **269**, 20250-20255
28. Roos, A., and Boron, W. F. (1981) *Physiol Rev* **61**, 296-434
29. Milton, A. E., and Weiner, I. D. (1998) *Am J Physiol* **274**, F1086-1094
30. Flessner, M. F., Wall, S. M., and Knepper, M. A. (1992) *Am J Physiol* **262**, F1-7

31. Zhelyaskov, V. R., Liu, S., and Broderick, M. P. (2000) *Kidney Int* **57**, 1764-1769
32. Hansen, G. M., Markesich, D. C., Burnett, M. B., Zhu, Q., Dionne, K. M., Richter, L. J., Finnell, R. H., Sands, A. T., Zambrowicz, B. P., and Abuin, A. (2008) *Genome Res* **18**, 1670-1679
33. Verlander, J. W., Miller, R. T., Frank, A. E., Royaux, I. E., Kim, Y. H., and Weiner, I. D. (2003) *Am J Physiol Renal Physiol* **284**, F323-337
34. Kim, H. Y., Verlander, J. W., Bishop, J. M., Cain, B. D., Han, K. H., Igarashi, P., Lee, H. W., Handlogten, M. E., and Weiner, I. D. (2009) *Am J Physiol Renal Physiol*
35. Kikeri, D., Sun, A., Zeidel, M. L., and Hebert, S. C. (1989) *Nature* **339**, 478-480
36. Bleich, M., Kottgen, M., Schlatter, E., and Greger, R. (1995) *Pflugers Arch* **429**, 345-354
37. Wall, S. M., and Koger, L. M. (1994) *Am J Physiol* **267**, F660-670
38. Wall, S. M., and Fischer, M. P. (2002) *J Am Soc Nephrol* **13**, 827-835
39. Gruswitz, F., Chaudhary, S., Ho, J. D., Schlessinger, A., Pezeshki, B., Ho, C. M., Sali, A., Westhoff, C. M., and Stroud, R. M. (2010) *Proc Natl Acad Sci U S A* **107**, 9638-9643
40. Mouro-Chanteloup, I., Cochet, S., Chami, M., Genetet, S., Zidi-Yahiaoui, N., Engel, A., Colin, Y., Bertrand, O., and Ripoche, P. (2010) *PLoS One* **5**, e8921
41. Jones, E. R., Beck, T. R., Kapoor, S., Shay, R., and Narins, R. G. (1984) *J Clin Invest* **74**, 992-1002
42. Prabhakar, S. S. (2004) *Kidney Int* **66**, 1742-1754
43. Wall, S. M., Fischer, M. P., Kim, G. H., Nguyen, B. M., and Hassell, K. A. (2002) *Am J Physiol Renal Physiol* **282**, F91-102
44. Bishop, J. M., Verlander, J. W., Lee, H. W., Nelson, R. D., Weiner, A. J., Handlogten, M. E., and Weiner, I. D. (2010) *Am J Physiol Renal Physiol* **299**, F1065-1077

FOOTNOTES

This study was supported by grants from the Swiss National Science Foundation to C.A. Wagner (3100A0-122217 and 31003A_138143), the 7th EU Frame work project EUNEFRON to P. Houillier, E.I. Christensen, O. Devuyst, and C.A. Wagner, The Danisk Medical Research Council and The Novo Nordisk Foundation to E.I. Christensen, and the Swiss National Centre of Competence in Research NCCR Kidney.CH to O. Devuyst and C.A. Wagner. The authors thank Yves Colin and Isabelle Mourot-Chanteloup for fruitful discussions. Hanne Siedelmann is thanked for skillful technical assistance. Suresh K Ramakrishnan is funded by Erasmus Mundus External Cooperation Window Lot 15 India.

The use of the Zurich Integrative Rodent Physiology (ZIRP) Core Facility is gratefully acknowledged.

FIGURE LEGENDS

Figure 1. *Rhcg* gene targeting and deletion. (A) *Rhcg* gene knock-out was achieved by replacement of exon 1 by a Lac Z/Neomycin cassette (TIGM, Houston, TX, USA). (**B)** RT-qPCR with primers placed in exon 1 of *Rhcg* demonstrated lower mRNA in kidneys from $Rhcg^{+/-}$ mice and absence of a detectable PCR product in kidneys from $Rhcg^{-/-}$ mice (n = 5 mice). (**C and D)** *Rhcg* immunodetection in kidney sections from (C) wild type and (D) *Rhcg-/-* mice. * significantly different $p < 0.05$.

Figure 2. Incomplete dRTA in $Rhcg^{+/-}$ and $Rhcg^{-/-}$ mice. Mice were observed in metabolic cages under basal conditions and during an acid load for up to 7 days with HCl added to the diet (n = 5-10 per genotype). $Rhcg^{-/-}$ could only be observed for 6 days during the HCl-containing diet since most animals had to be terminated earlier. **(A)** Urinary ammonium excretion in 24 hr urine collections normalized for urinary creatinine. **(B)** Urinary pH in 24 hrs urine collections. **(C)** Urinary net acid excretion (total bars) calculated from urinary ammonium (open bars) plus titratable acid (grey bars).

Urinary bicarbonate levels were measured and negligible. **(D)** Blood bicarbonate concentrations **(E)** Blood pH values.
* p<0.05 for *Rhcg*$^{-/-}$ versus *Rhcg*$^{+/+}$. ¥ p< 0.05 for *Rhcg*$^{+/-}$ versus *Rhcg*$^{+/+}$

Figure 3. Medullary ammonium accumulation is altered in *Rhcg*$^{-/-}$ mice. Kidneys from all three genotypes were dissected after 4 days of HCl-load. Cortex (C), outer medulla (OM) and inner medulla (IM) were separated and tissue ammonium content measured. In wildtype and heterozygous mice a gradient in renal tissue ammonia content from cortex to inner medulla was observed. In *Rhcg*$^{-/-}$ mice, the ammonia content increased from cortex to outer medulla, but ammonium content was lower in the inner medulla than in mice from the other 2 genotypes. (n = 5-8 mice/ genotype), * statistically different from *Rhcg*$^{+/+}$ mice ($p < 0.05$)

Figure 4. Rhcg immunodetection in mouse kidney and Immunogold electron microscopic localization of Rhcg in CCD.. A, B Rhcg protein immunodetection in mouse kidney cortex. *Rhcg* related staining was detected in the distal convoluted tubule (DCT) starting immediately at the transition from the thick ascending limb (TAL) to the DCT (arrow), in the connecting tubule (CNT) and cortical collecting duct (CCD). Most but not all cells are stained Rhcg staining is observed in most cells at the apical and basolateral sides but in some cells (arrow heads) only an apical signal is detected. **C** Rhcg immunodetection in outer medulla. Rhcg is strictly expressed in collecting ducts at both sides of intercalated and segment specific cells. **D** In the inner medulla, Rhcg is expressed only in intercalated cells. **E, F** Rhcg was detected both at the apical membrane (**E**) and at the invaginations of the basolateral membrane (**F**) of segment specific cells in the cortical collecting duct by gold immuno-electron microscopy.

Figure 5. Transepithelial NH_3 permeability is reduced in the cortical collecting duct from *Rhcg*$^{+/-}$ and *Rhcg*$^{-/-}$ mice. Transepithelial permeability to NH_3 was assessed in *in vitro* isolated and microperfused cortical collecting ducts from mice kept for 2 days on HCl diet by imposing a bath-to-lumen NH_3 gradient (see method section) (* p<0.05).

Figure 6. RhCG is required for apical NH_3 permeability of cortical collecting duct cells. Cortical collecting duct were isolated from kidneys of *Rhcg*$^{+/+}$, *Rhcg*$^{+/-}$ and *Rhcg*$^{-/-}$ mice after 2 days of HCl-loading and intracellular pH monitored with BCECF. 20 mM NH_4Cl was applied with the luminal perfusate. **(A)** pHi recording from CCD exposed to a luminal NH_4Cl pulse in *Rhcg*$^{+/+}$ and *Rhcg*$^{+/-}$ CCD . Exposure to NH_4Cl caused a rapid alkalinization corresponding to NH_3 entry into cells. The initial slopes ($\Delta pHi/\Delta t$) of the alkalinization phase was measured and the amount of NH_3 titrated into NH_4^+ was finally calculated based on intracellular buffering power. **(B)** Bar graph summarizing the amount of titrated NH_3 during luminal NH_4Cl pulses (n = 8-12 tubules/genotype).

Figure 7. Basolateral NH_3 permeability of cortical collecting duct cells. Cortical collecting duct were isolated from kidneys of *Rhcg*$^{+/+}$ *Rhcg*$^{+/-}$ and *Rhcg*$^{-/-}$ mice after 2 days of HCl-loading and intracellular pH monitored with BCECF. After an equilibrium phase, 6 mM NH_4Cl was applied to the bath. Exposure to NH_4Cl caused a rapid alkalinization corresponding to NH_3 entry into cells. The initial slopes ($\Delta pHi/\Delta t$) of the alkalinization phase was measured and the amount of NH_3 titrated into NH_4^+ was finally calculated based on intracellular buffering power. The bar graph summarizes the amount of titrated NH_3 (alkalinization phase) during basolateral NH_4Cl pulses (n = 5-7 tubules/genotype).

Figure 8. Deletion of *Rhcg* affects the abundance of proteins involved in ammoniagenesis and ammonium transport. Crude membrane and cytosolic fractions were prepared from total kidneys from *Rhcg*$^{+/+}$, *Rhcg*$^{+/-}$ and *Rhcg*$^{-/-}$ mice after 2 days of HCl-loading, 40 µg loaded on SDS page and their abundance tested. **(A)** phospho-enol puyruvate carboxy kinase (PEPCK), **(B)** phosphate-dependent glutaminase (PDG) **(C)** the Na^+-K^+-$2Cl^-$ cotransporter isoform 2 (NKCC2), and **(D)** the Na^+/ H^+ exchanger isoform 3 (NHE3). All membranes were stripped and reprobed for β-actin to control for loading. Bar graphs summarize results from densitometric analysis of proteins of interest

normalized against β-actin. N = 5 mice/ genotype. * statistically significant, $p < 0.05$ versus $Rhcg^{+/+}$ tissue

Table 1. Blood values in *Rhcg* littermates mice under normal diet and during an acid load

	Basal status			2 days HCl			7 days HCl		
	$Rhcg^{+/+}$ (n=10)	$Rhcg^{+/-}$ (n=16)	$Rhcg^{-/-}$ (n=9)	$Rhcg^{+/+}$ (n=10)	$Rhcg^{+/-}$ (n=10)	$Rhcg^{-/-}$ (n=9)	$Rhcg^{+/+}$ (n=12)	$Rhcg^{+/-}$ (n=21)	$Rhcg^{-/-}$ (n=2)
pH	7.38 ± 0.02	7.38 ± 0.02	7.28 ± 0.04	7.17 ± 0.02*	7.17 ± 0.02*	7.07 ± 0.02$^{\#}$*	7.24 ± 0.03*	7.17 ± 0.02$^{\#}$*	6.88 ± 0.07
pCO_2 (mmHg)	34.0 ± 1.3	37.2 ± 0.9	38.8 ± 1.4$^{\#}$	41.2 ± 2.0*	39.4 ± 0.7	37.8 ± 0.9	42.0 ± 1.4*	40.0 ± 0.8	44.6 ± 1.6
HCO_3 (mM)	19.0 ± 1.1	22.4 ± 1.0	18.3 ± 2.1	14.3 ± 0.6*	13.8 ± 0.5*	11.1 ± 0.6$^{\#}$*	18.6 ± 1.3	13.9 ± 0.6$^{\#}$*	7.9 ± 1.05
pO_2	74.7 ± 9.7	52.3 ± 3.4	63.6 ± 6.3	60.1 ± 2.3	59.4 ± 1.4	65.7 ± 4.1	57.1 ± 3.0	63.1 ± 3.4	82.3 ± 4.6
Na (mM)	143.9 ± 1.5	145.4 ± 0.9	148.0 ± 0.4	150.1 ± 1.0	145.8 ± 0.8	150.4 ± 0.9	148.3 ± 0.6	149.1 ± 0.5	148.5 ± 1.5
Cl (mM)	117.5 ± 1.9	112.1 ± 1.7	111.7 ± 1.5	123.7 ± 1.0*	119.7 ± 1.0*	126.4 ± 0.9*	118.9 ± 0.9	122.6 ± 0.7$^{\#}$*	134.0 ± 0.0
Ionized Ca (mM)	1.23 ± 0.02	1.25 ± 0.01	1.29 ± 0.03	1.41 ± 0.03*	1.35 ± 0.01*	1.42 ± 0.02*	1.34 ± 0.01*	1.37 ± 0.01$^{\#}$*	1.01 ± 1.9
Glucose (mM)	10.6 ± 0.7	10.9 ± 0.5	10.8 ± 0.8	7.8 ± 0.4*	9.0 ± 0.3$^{\#}$	6.5 ± 0.4$^{\#}$*	9.6 ± 0.4	8.8 ± 0.3*	*ND*
Hb (g/dl)	15.0 ± 1.1	15.7 ± 0.3	16.3 ± 0.5	16.3 ± 0.4	15.5 ± 0.3	17.5 ± 0.3$^{\#}$*	15.2 ± 0.5	14.9 ± 0.4	17.4 ± 1.0

* $p<0.05$ versus baseline period in same genotype, $^{\#}$ $p<0.05$ versus $Rhcg^{+/+}$ mice during the same period.

Table 2. Weight, food intake and urinary values in *Rhcg* littermates mice under normal diet and a 2 days HCl load

	Basal status			2 days HCl		
	Rhcg$^{+/+}$ (n = 14)	*Rhcg*$^{+/-}$ (n = 13)	*Rhcg*$^{-/-}$ (n = 13)	*Rhcg*$^{+/+}$ (n = 14)	*Rhcg*$^{+/-}$ (n = 13)	*Rhcg*$^{-/-}$ (n = 13)
Weight (g)	26.4 ± 0.6	28.7 ± 1.2	27.6 ± 1.0	24.9 ± 0.5	26.6 ± 0.8	25.0 ± 1.1
Weight lose in % of body weight under basal status	*ND*	*ND*	*ND*	8,3 ± 0.4	11.4 ± 1.3	15.0 ± 1.0$^{\#}$
Food intake (g/24hrs/body weight)	0.31 ± 0.06	0.26 ± 0.02	0.26 ± 0.02	0.24 ± 0.01	0.21 ± 0.01	0.21 ± 0.02
Urine values						
volume (ml/24 h)	1.9 ± 0.2	2.0 ± 0.1	1.9 ± 0.1	2.5 ± 0.3	2.1 ± 0.2	2.1 ± 0.4*
creatinine excretion (µmol/24 h)	7.6 ± 0.3	6.2 ± 0.6	7.8 ± 0.4	7.5 ± 0.7	5.6 ± 1.4	8.3 ± 2.3
Urinary pH	6.13 ± 0.04	6.18 ± 0.06	6.03 ± 0.06	5.47 ± 0.05*	5.44 ± 0.02*	5.68 ± 0.06$^{\#}$*
UNH_4/UCr (mEq/mmol)	4.6 ± 1.0	5.1 ± 0.7	4.1 ± 1.0	37.8 ± 4.1*	43.8 ± 6.0*	11.1 ± 1.5$^{\#}$*
UTA/UCr (mEq/mmol)	15.4 ± 1.2	14.4 ± 1.0	13.6 ± 1.1	20.9 ± 2.5	15.9 ± 3.2	14.5 ± 1.9
UPi/UCr (mEq/mmol)	16.1 ± 1.7	20.3 ± 1.0	17.7 ± 1.4	9.3 ± 1.5	10.7 ± 1.7	8.2 ± 1.6
Uurea/UCr (mg/mmol)	266.3 ± 14.8	279.3 ± 14.8	280.8 ± 15.0	229.2 ± 17.1	255.1 ± 24.01	146.8 ± 15.7$^{\#}$*
UNA/UCr (mEq/mmol)	20.0 ± 1.4	19.4 ± 0.8	17.7 ± 1.3	58.7 ± 4.9*	60.9 ± 9.0*	25.6 ± 2.9$^{\#}$*
UNa/UCr (mEq/mmol)	16.8 ± 2.0	10.0 ± 2.0	15.5 ± 2.0	15.4 ± 1.6	15.8 ± 3.6	9.7 ± 1.7
UCl/UCr (mEq/mmol)	32.8 ± 2.0	30.6 ± 1.7	32.6 ± 2.3	133.0 ± 14.4*	132.3 ± 19.8*	40.5 ± 9.2$^{\#}$*
UK/UCr (mEq/mmol)	60.1 ± 3.9	60.2 ± 4.6	63.1 ± 4..9	53.9 ± 4.3	56.3 ± 7.3	27.7 ± 3.2

* $p<0.05$ versus baseline period in same genotype, $^{\#}$ $p<0.05$ versus *Rhcg*$^{+/+}$ mice during the same period. TA: Titratable Acid; NA: Net Acid

Table 3. Weight, food intake and urinary values in 3-month old *Rhcg*$^{+/+}$, *Rhcg*$^{+/-}$ littermates during 6 or 7 days HCl load

	6 days HCl			7 days HCl	
	Rhcg$^{+/+}$ (n = 8)	*Rhcg*$^{+/-}$ (n = 10)	*Rhcg*$^{-/-}$ (n = 2)	*Rhcg*$^{+/+}$ (n = 8)	*Rhcg*$^{+/-}$ (n = 10)
Weight (g)	*ND*	*ND*	19.6 - 22.4	25.1 ± 1.2	23.3 ± 0.8*
Weight lose in % of body weight under basal status	*ND*	*ND*	*ND*	*10.0 ± 1.1 (n=5)*	14.8 ± 2.1 (n = 5)
Food intake (g/24hrs/body weight)	*ND*	*ND*	0.31 - 0.44	0.37 ± 0.03	0.39 ± 0.02
Urine values					
volume (ml/24 h)	3.8 ± 0.8*	4.4 ± 0.8*	2.5 - 2.6	3.1 ± 0.2*	3.9 ± 0.1*
creatinine excretion (µmol/24 h)	8.5 ± 2.0	7.2 ± 1.8	3.8 - 4.3	6.6 ± 0.3	7.9 ± 1.4
Urinary pH	5.39 ± 0.13*	5.59 ± 0.07*	5.20 - 5 .52	5.57 ± 0.02*	5.73 ± 0.05$^{\#}$*
UNH_4/UCr (mEq/mmol)	153.9 ± 31.1*	173.1 ± 20.6*	17.3 - 36.3	147.4 ± 26.3*	171.8 ± 22.3*
UTA/UCr (mEq/mmol)	25.4 ± 2.6*	17.9 ± 2.5	28.6 - 36.2	26.3 ± 0.6*	16.6 ± 0.7$^{\#}$
UPi/UCr (mEq/mmol)	ND	ND	ND	9.8 ± 3.7	25.0 ± 8.8
UNA/UCr (mEq/mmol)	131.2 ± 6.3*	128.5 ± 16.4*	68.9 - 53.4	126.8 ± 9.8	118.3 ± 15.0
Uurea/UCr (mg/mmol)	205.2 ± 11.2*	220.3 ± 9.9*	186.4 - 230.1	208.9 ± 6.3*	220.6 ± 5.5*
UNa/UCr (mEq/mmol)	36.9 ± 3.8*	32.9 ± 2.8*	67.4 - 70.9	43.0 ± 3.0*	38.4 ± 4.0*
UCl/UCr (mEq/mmol)	242.6 ± 11.2*	253.6 ± 11.4*	135.1 - 173.1	269.5 ± 12.0*	263.5 ± 14.9*
UK/UCr (mEq/mmol)	77.6 ± 4.2	79.7 ± 4.1	19.6 - 22.4	92.2 ± 2.0	85.2 ± 9.9

* $p<0.05$ versus baseline period in same genotype, $^{\#}$ $p<0.05$ versus *Rhcg*$^{+/+}$ mice during the same period. TA: Titratable Acid; NA: Net Acid

Table 4. Summary of RhCG localization along the mouse nephron

	Tubule type	Cell type	Localization	staining intensity
Cortex	DCT		apical	high
			basolateral	weak
	CNT	principal cells	plasma membrane	high
		intercalated cells	plasma membrane/apical	high
	CCD	principal cells	plasma membrane	high
		intercalated cells	plasma membrane/apical	high
Outer Medulla	OMCD	principal cells		
		intercalated cells	plasma membrane/apical	high
Inner Medulla	IMCD	principal cells	no staining	
		intercalated cells	Plasma membrane/apical	weak/high

Table 5. *CCD in vitro microperfusion data from $Rhcg^{+/+}$, $Rhcg^{+/-}$ and $Rhcg^{-/-}$ mice*

	$Rhcg^{+/+}$ (n = 7)	$Rhcg^{+/-}$ (n = 9)	$Rhcg^{-/-}$ (n = 5)
Tubule length, mm	0.38 ± 0.04	0.36± 0.05	0.034 ± 0.08
Tubule diameter, µm	54.98 ± 4.55	47.92 ± 4.24	44.31 ± 8.88
Collection rate, $nl \cdot mm^{-1} \cdot min^{-1}$	4.61 ± 0.22	4.37 ± 0.29	3.96 ± 0.42
Perfusate pH	6.44 ± 0.04	6.37 ± 0.04	6.50 ± 0.04
Bath pH	7.42 ± 0.03	7.37 ± 0.03	7.38 ± 0.03
Total ammonia perfusate, mM	1.41 ± 0.08	1.40 ± 0.08	1.42 ± 0.13
$[NH_3]$ perfusate, µM	3.74 ± 0.37	3.30 ± 0.32	4.16 ± 0.25
Total ammonia bath, mM	1.41 ± 0.08	1.40 ± 0.08	1.42 ± 0.13
$[NH_3]$ bath, µM	34.38 ± 3.26	32.57 ± 3.72	31.39 ± 3.71
Total ammonia collected, mM	3.88 ± 0.42	2.47 ± 0.36	1.48 ± 0.35
$[NH_3]$ collected, µM	10.37 ± 1.45	5.90 ± 1.24*	4.25 ± 0.93*
Total ammonia flux, $pmol \cdot mm^{-1} \cdot min^{-1}$	32.98 ± 3.32*	17.84 ± 4.56*	2.51 ± 3.51*
NH_3 permeability, mm/s	0.13 ± 0.02	0.08 ± 0.02*	0.02 ± 0.02*

Values are mean ± SE; *n,* no. of mice; CCD, cortical collecting duct. * $p<0.05$ versus control mice

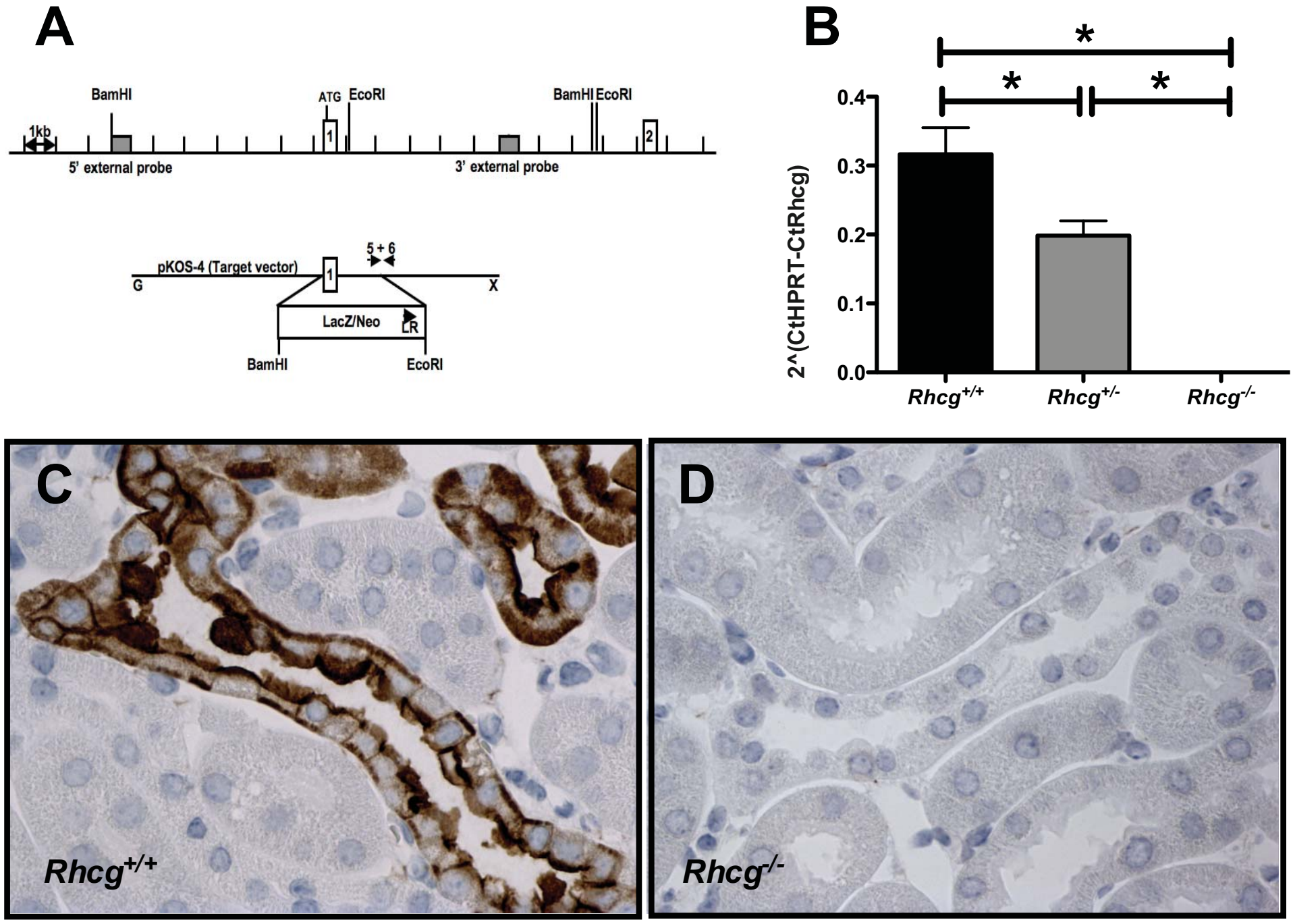
A
BamHI
ATG EcoRI
BamHI EcoRI
1kb
1
2
5' external probe
3' external probe
pKOS-4 (Target vector)
5 + 6
1
G
X
LacZ/Neo
LR
BamHI
EcoRI
B
*
*
*
0.4
0.3
0.2
0.1
0.0
2^(CtHPRT-CtRhcg)
Rhcg+/+
Rhcg+/-
Rhcg-/-
C
Rhcg+/+
D
Rhcg-/-

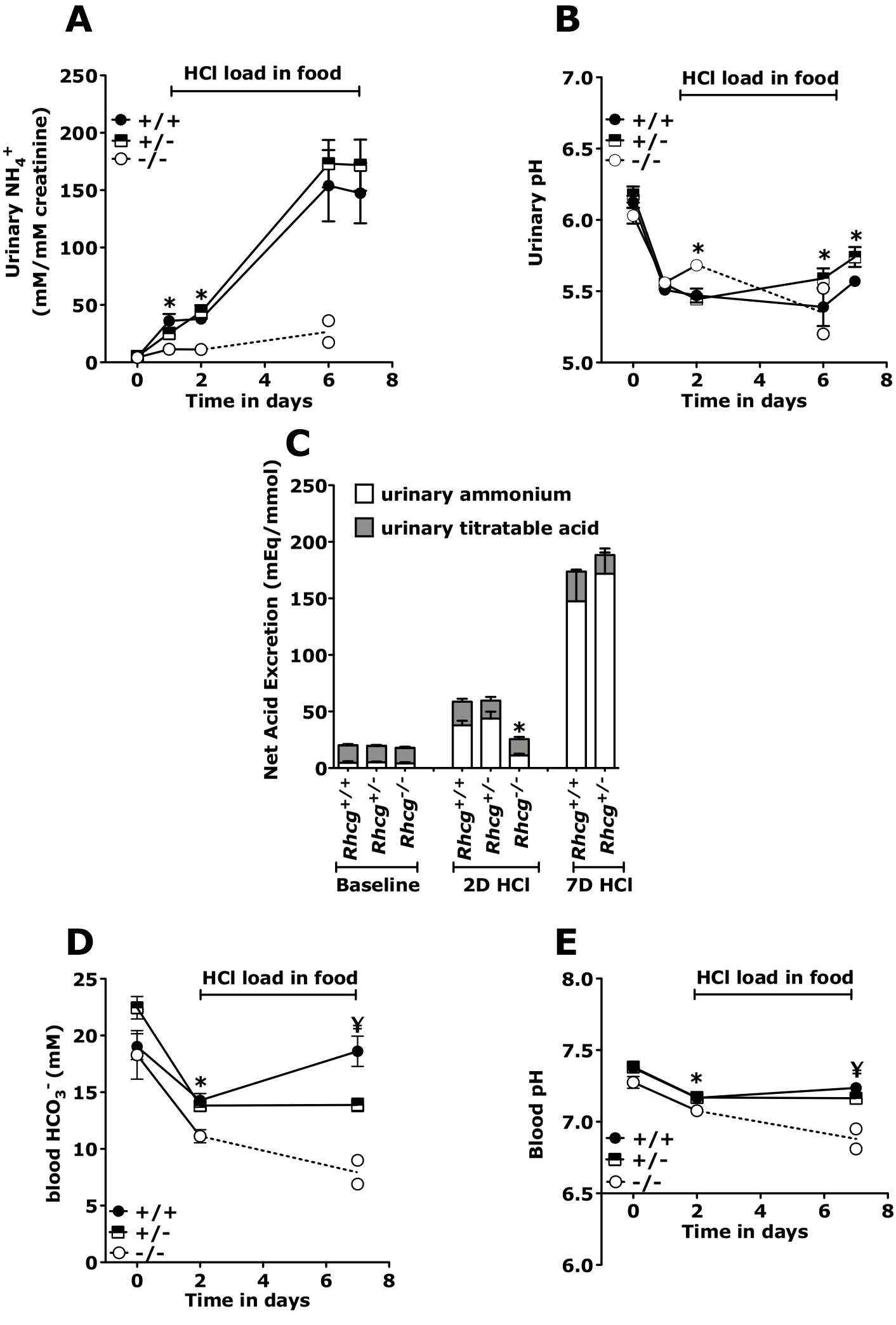
A
HCl load in food
+/+
+/-
-/-
Urinary NH_4^+ (mM/mM creatinine)
Time in days
B
HCl load in food
Urinary pH
Time in days
C
urinary ammonium
urinary titratable acid
Net Acid Excretion (mEq/mmol)
Rhcg+/+
Rhcg+/-
Rhcg-/-
Baseline
2D HCl
7D HCl
D
HCl load in food
blood HCO_3^- (mM)
Time in days
E
HCl load in food
Blood pH
Time in days

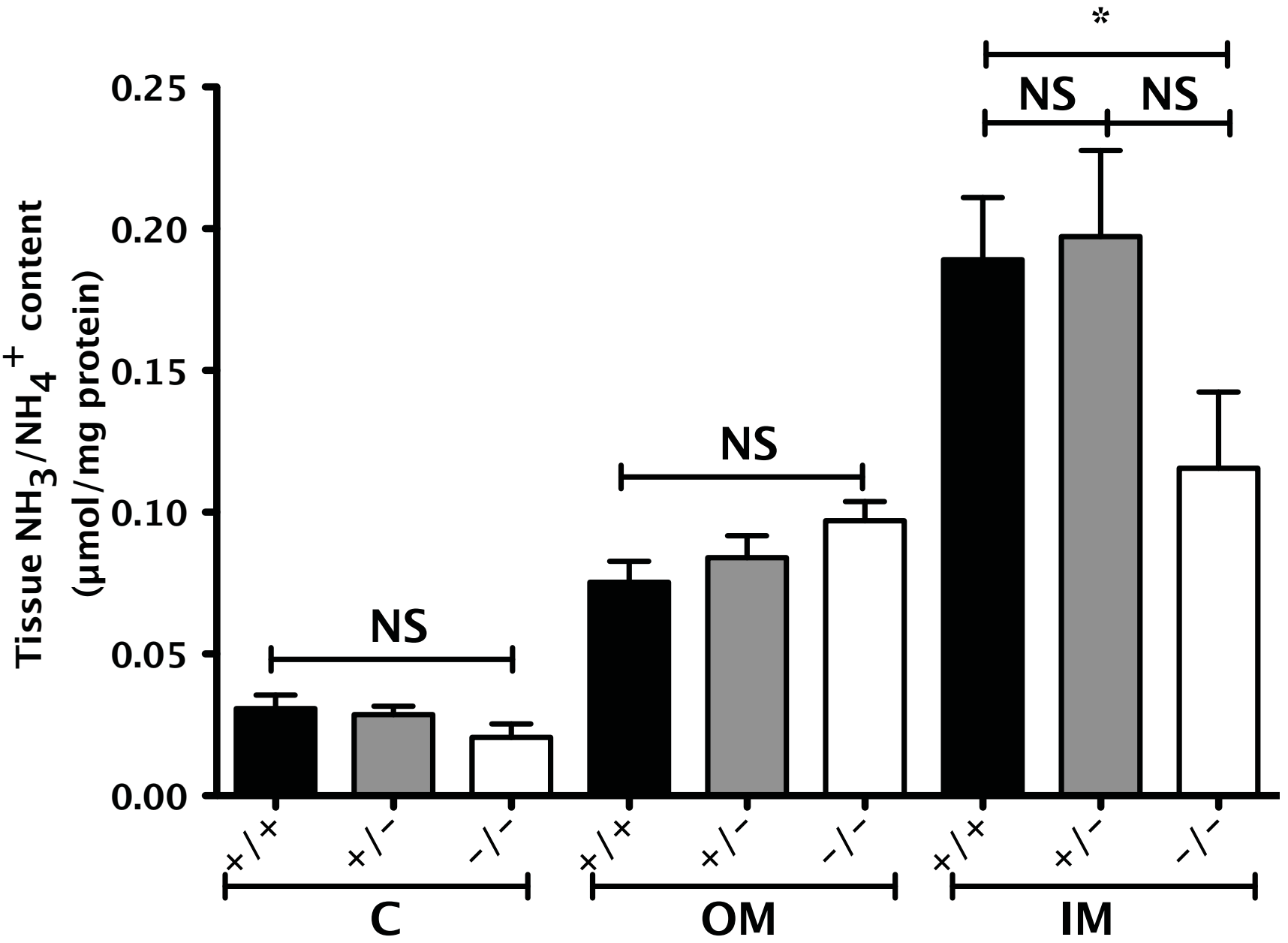
*
NS
NS
NS
NS
0.25
0.20
0.15
0.10
0.05
0.00
Tissue NH3/NH4+ content
(µmol/mg protein)
+/+
+/−
−/−
+/+
+/−
−/−
+/+
+/−
−/−
C
OM
IM

Figure 4

Bourgeois et al.

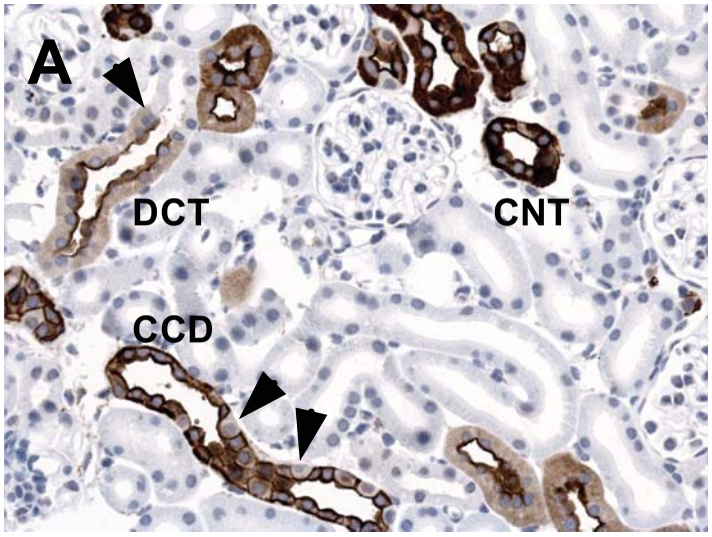

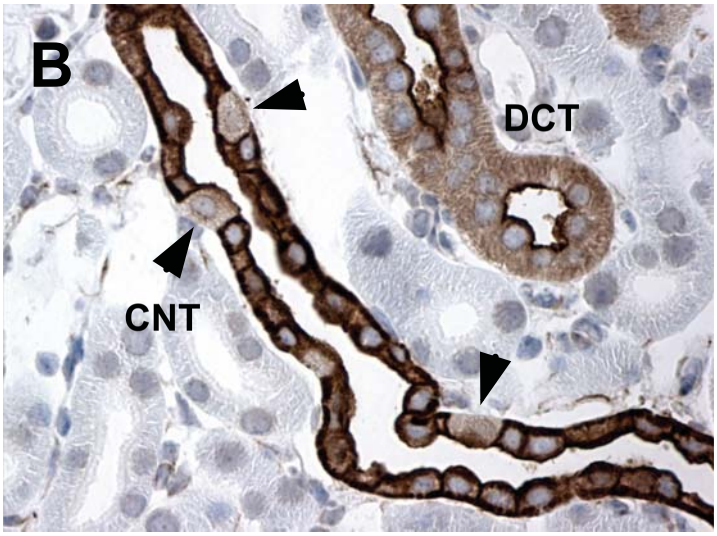

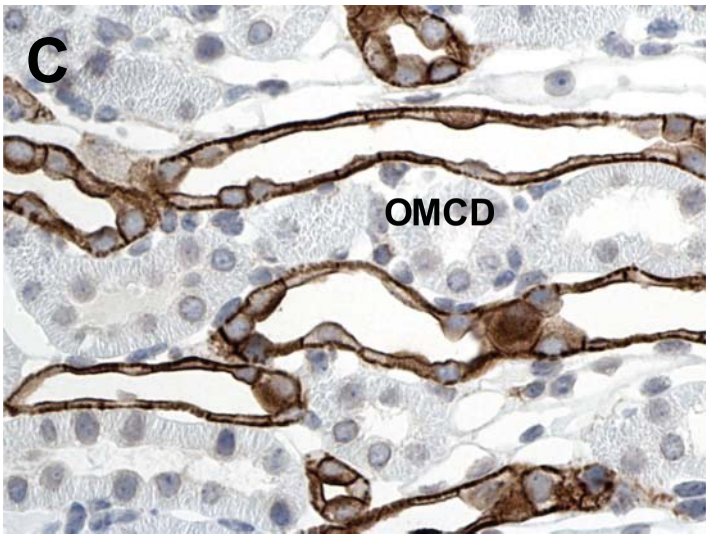

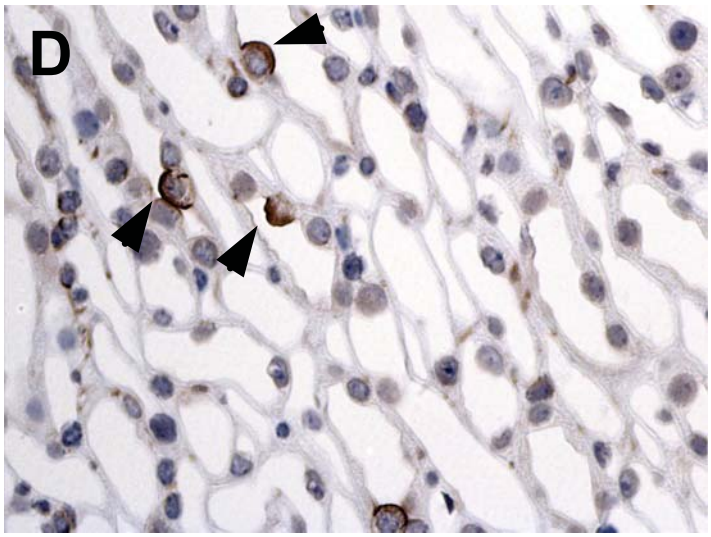

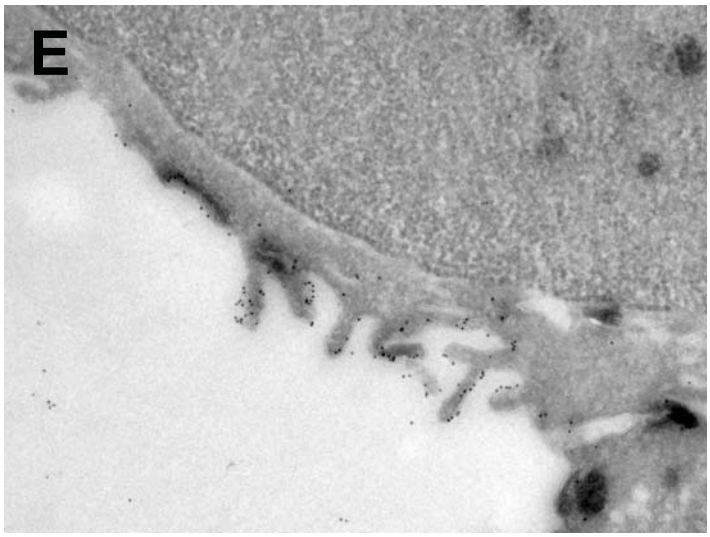

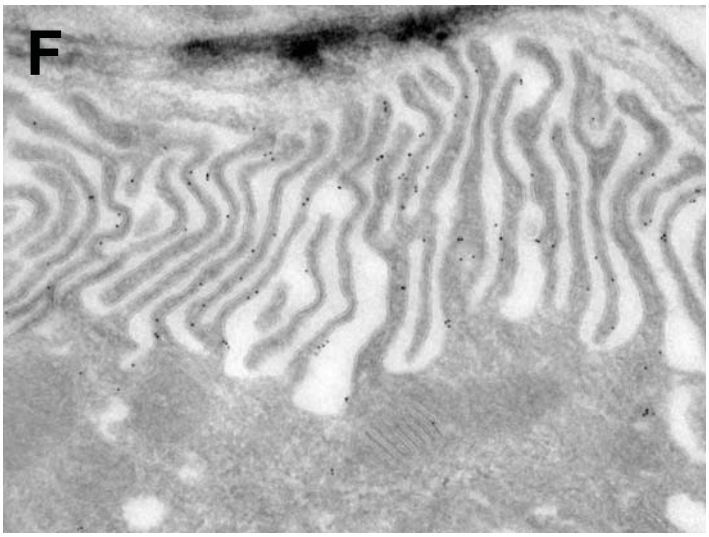

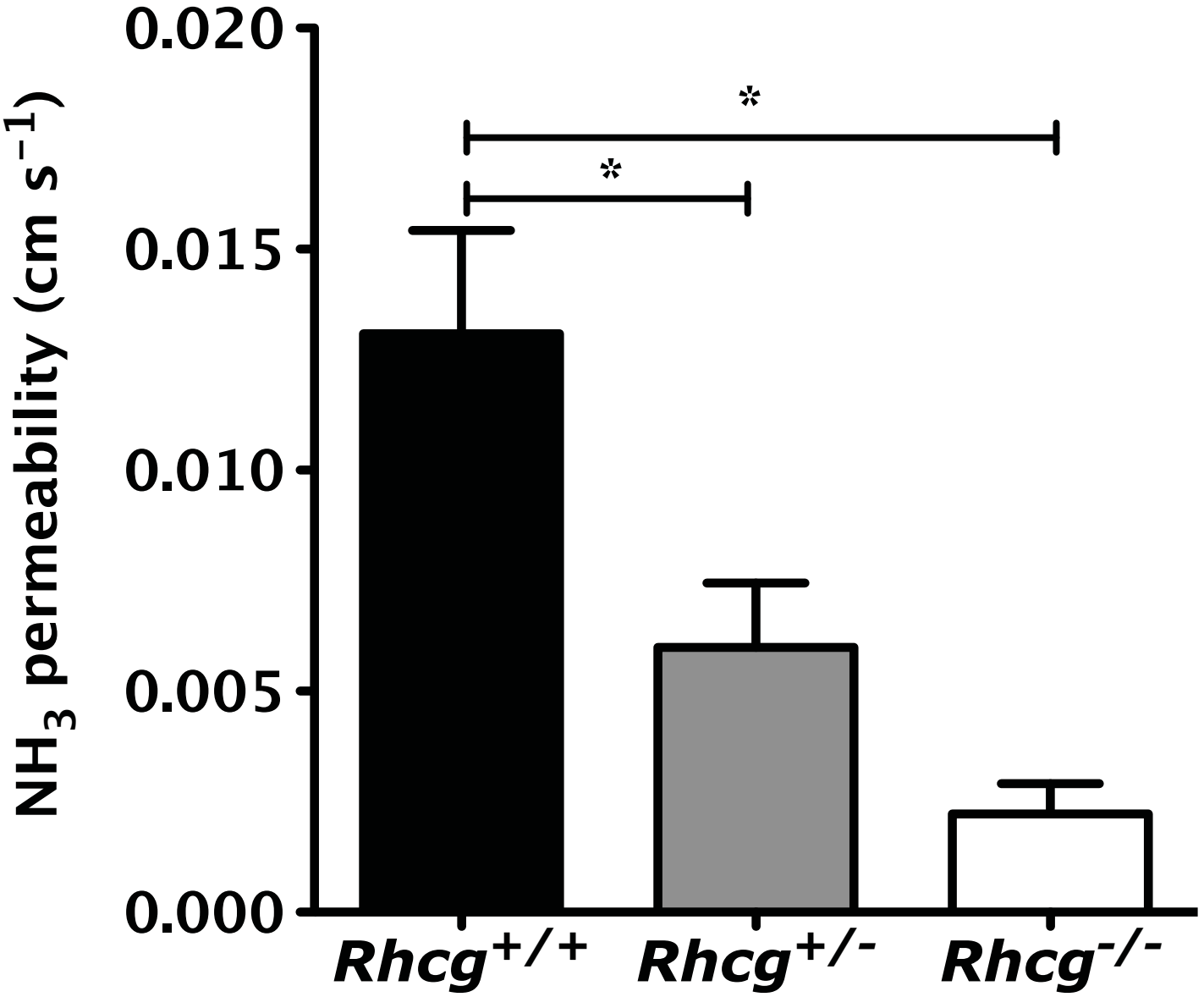
0.020
0.015
0.010
0.005
0.000
NH_3 permeability (cm s^{-1})
*
*
Rhcg+/+
Rhcg+/-
Rhcg-/-

Figure 6

Bourgeois et al.

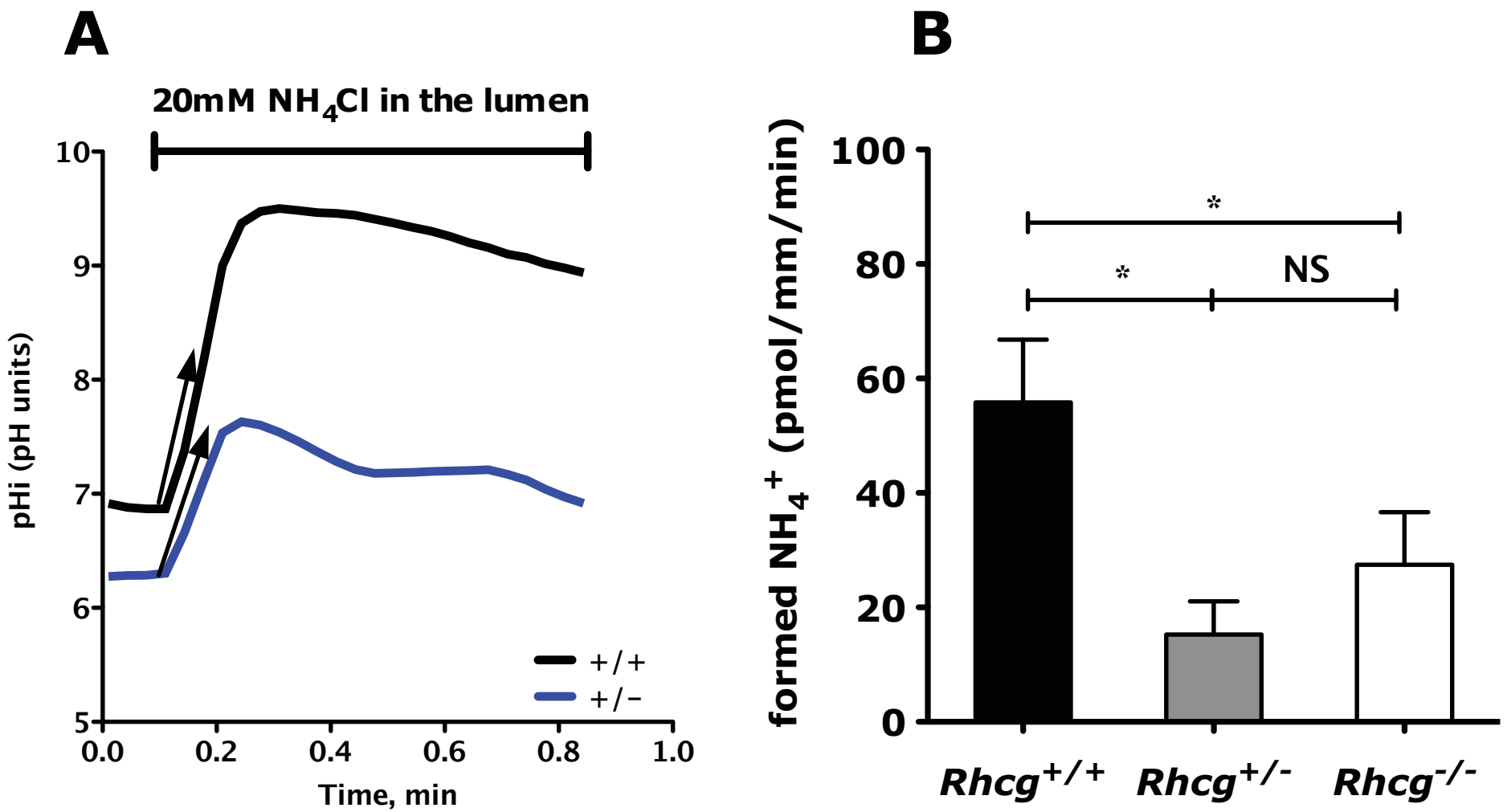

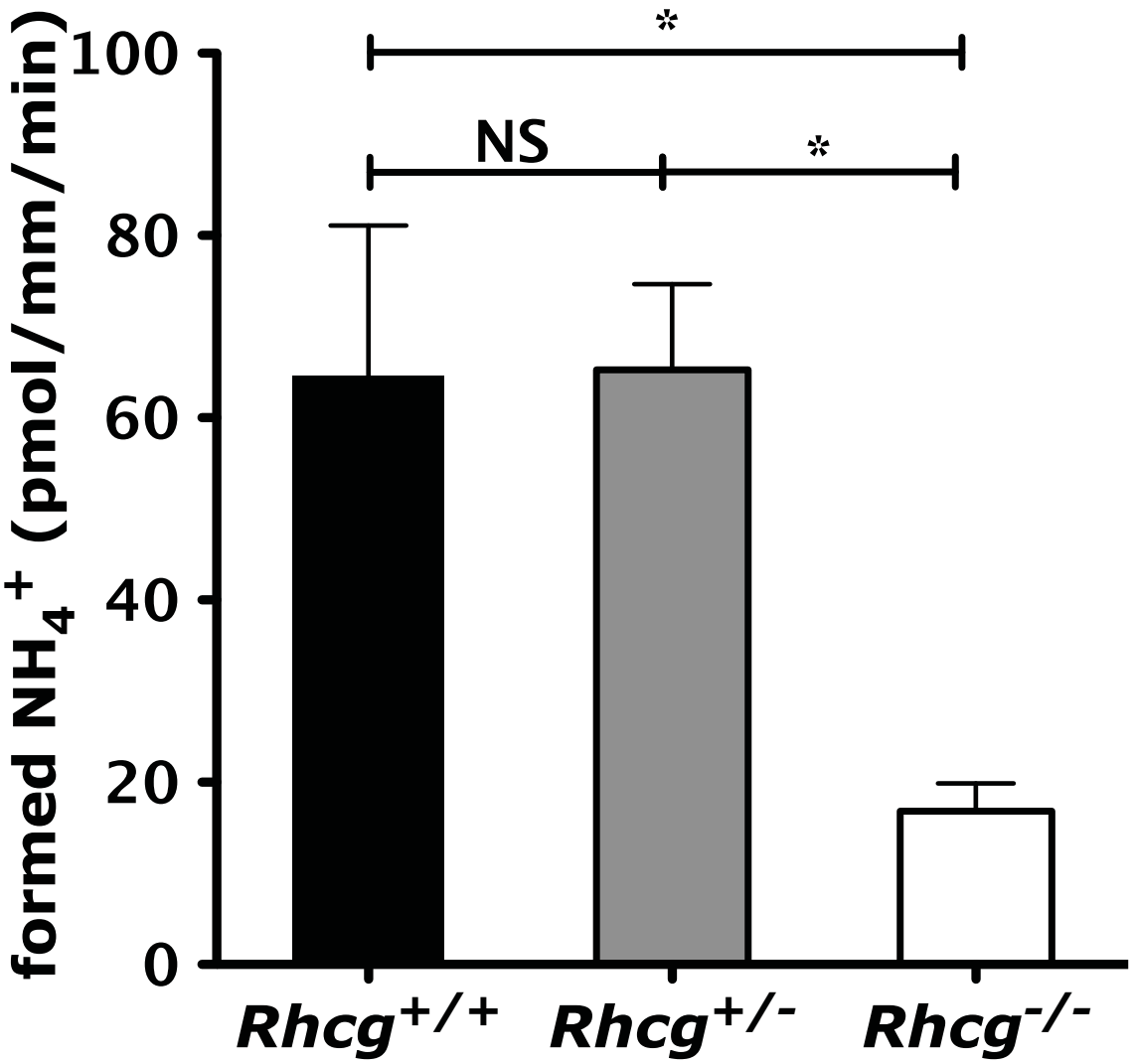
*
NS
*
100
80
60
40
20
0
formed NH_4^+ (pmol/mm/min)
Rhcg+/+
Rhcg+/-
Rhcg-/-

Figure 8

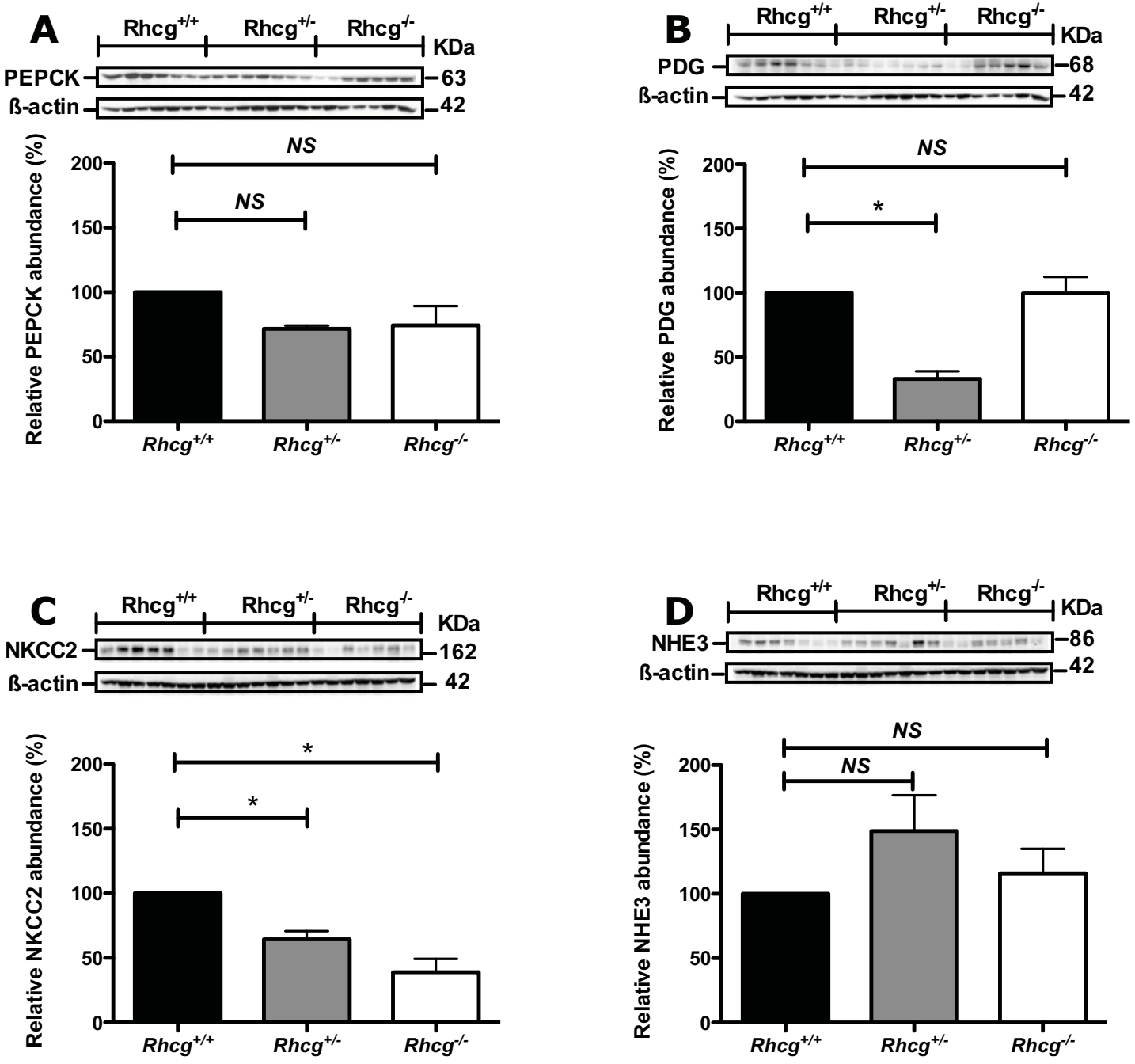
A
Rhcg+/+
Rhcg+/-
Rhcg-/-
KDa
PEPCK
63
ß-actin
42
Relative PEPCK abundance (%)
NS
NS
200
150
100
50
0
Rhcg+/+
Rhcg+/-
Rhcg-/-
B
Rhcg+/+
Rhcg+/-
Rhcg-/-
KDa
PDG
68
ß-actin
42
Relative PDG abundance (%)
NS
*
200
150
100
50
0
Rhcg+/+
Rhcg+/-
Rhcg-/-
C
Rhcg+/+
Rhcg+/-
Rhcg-/-
KDa
NKCC2
162
ß-actin
42
Relative NKCC2 abundance (%)
*
*
200
150
100
50
0
Rhcg+/+
Rhcg+/-
Rhcg-/-
D
Rhcg+/+
Rhcg+/-
Rhcg-/-
KDa
NHE3
86
ß-actin
42
Relative NHE3 abundance (%)
NS
NS
200
150
100
50
0
Rhcg+/+
Rhcg+/-
Rhcg-/-